

Development of a Laser Cooling and Magneto-Optical Trapping Experiment for Rubidium 87 Atoms

by

Charles Ian Rigby

*Thesis presented in partial fulfillment of the
requirements for the degree of Masters of Laser Physics*



at

Stellenbosch University

Department of Physics

Faculty of Science

Supervisor: Dr. Christine M. Steenkamp
Co-supervisor: Prof. Erich G. Rohwer

Date: March 2011

Declaration

By Submitting this thesis electronically, I declare that the entirety of the work contained therein is my own, original work, that I am the owner of the copyright thereof (save to the extent explicitly otherwise stated), that reproduction and publication thereof by Stellenbosch University will not infringe any third party rights and that I have not previously in its entirety or in part submitted it for obtaining any qualification.

Date: 28 February 2011

Copyright © 2011 Stellenbosch University

All rights reserved

Abstract

A magneto optical trap (MOT) is capable of trapping a vapor cloud consisting of atoms cooled down to the micro Kelvin range. Three orthogonal pairs of counter-propagating laser beams of the correct circular polarisation form an optical molasses which facilitates the cooling of neutral atoms. Additionally a spatially non-uniform magnetic field produced by two current carrying coils in a Maxwell gradient configuration is used to trap the cooled atoms. In this report the effects of the trap parameters, including the laser beam intensity and frequency detuning, beam diameter and magnetic field gradient, on the number of trapped atoms are discussed. Secondly the development of an experimental setup for laser cooling and trapping of ^{87}Rb atoms in vacuum with the aid of a MOT is presented. All trap components were implemented and characterised. The vacuum system and trapping chamber in which the cooling takes place were designed and constructed. A rubidium getter to act as a source of atoms was integrated into the vacuum system. The two external cavity diode lasers used for trapping and optical re-pumping were characterised. The optical setup required for the optical molasses was designed, constructed and characterised. Saturated absorption spectroscopy was performed to investigate the hyperfine structure of ^{87}Rb and to frequency lock the lasers. We report on the current status of the project with regards to progress, results and future work.

Opsomming

'n Magneto-optiese val (magneto optical trap, MOT) kan 'n dampwolk van atome vang en afkoel tot in die mikro Kelvin bereik. Drie ortogonale pare laserbundels, elke paar voortplantend in teenoorgestelde rigtings, met die korrekte sirkelvormige polarisasie vorm 'n sogenaamde optiese molasse wat die afkoeling van neutrale atome moontlik maak. Bykomend word 'n ruimtelik nie-uniforme magneetveld geproduseer deur twee stroomdraende spoele in 'n Maxwell gradient-opstelling gebruik om die afgekoelde atome te vang. In hierdie verslag word die invloed van die val parameters, insluitend die laserbundel intensiteit en frekwensie afstemming, die laserbundel deursnit en magneetveld gradiënt, op die aantal atome in die val bespreek. Tweedens word die ontwikkeling van 'n eksperimentele opstelling vir laser afkoeling en vang van ^{87}Rb atome in vakuum met die hulp van 'n MOT voorgelê. Alle komponente van die val is geïmplementeer en gekarakteriseer. Die vakuumsisteem en val-kamer waarin die afkoeling plaasvind is ontwerp en gebou. 'n Rubidium gasbinder is in die vakuumsisteem ingebou om as 'n bron van atome te dien. Die twee eksterne resonator diodelasers wat gebruik is vir die val en die optiese terugpomp is gekarakteriseer. Die optiese opstelling wat nodig is vir die optiese molasse is ontwerp, gebou en gekarakteriseer. Versadigde absorpsiespektroskopie is uitgevoer om die hiperfynstruktuur van ^{87}Rb te ondersoek en om die lasers se frekwensies te stabiliseer. Verslag word gedoen oor die huidige stand van die projek wat betref vordering, resultate en toekomstige werk.

Acknowledgments

I would like to thank:

1. Dr. C.M. Steenkamp and Prof. E.G. Rohwer, my supervisors on this project, for their constructive help and guidance.
2. The physics department workshop staff for construction of my various designs and providing expert advice during the design process.
3. Mr E. Ward, the Stellenbosch University glass blower, for assistance in making the trapping cells which were used.
4. Mr E. Shields, for construction of numerous electronics required in the workings of the setup.
5. The National Research Foundation for providing funding enabling me to spend the time to conduct this research project.
6. All the members of the Laser Research Institute at Stellenbosch University for their various contributions and encouragement.
7. My friends and family who have supported me throughout this process.

Contents

Contents	i
List of Figures	iii
List of Tables	vi
1 INTRODUCTION	1
1.1 Motivation	1
1.2 Aims	2
2 LITERATURE REVIEW AND PRINCIPLES OF TECHNIQUES EMPLOYED	3
2.1 Spectral Line Broadening	3
2.2 Properties of Rubidium	4
2.2.1 Energy level splittings	5
2.3 Principles of Laser Cooling and Magneto Optical Trapping	7
2.4 Parameters Influencing the Number of Trapped Atoms	12
2.5 Literature on Magneto Optical Trap Setups.	15
2.5.1 External cavity diode lasers	15
2.5.2 Saturated absorption spectroscopy and frequency locking	16
2.5.3 Vacuum system and atomic rubidium source	17
2.5.4 Optical setup for an optical molasses	18
2.5.5 Magnetic field coils	18
3 EXPERIMENTAL SETUP	19
3.1 Overview	19
3.2 External Cavity Diode Lasers	19
3.3 Saturated Absorption Spectroscopy and Frequency Locking	20
3.4 Vacuum System and Rubidium Source	21
3.5 Optical Setup for an Optical Molasses	22
3.6 Magnetic Field Coils	23
4 RESULTS AND DISCUSSION	25
4.1 Characterisation of External Cavity Diode Lasers	25
4.2 Optical Setup Characterisation	27
4.2.1 Optical power	27
4.2.2 Polarisation	27
4.3 Magnetic Field Characterisation	30
4.4 Saturated Absorption Spectra of Rubidium	32
4.5 Results on Frequency Locking of External Cavity Diode Lasers	33

4.6	Magneto Optical Trap Operation	36
5	SUMMARY, CONCLUSIONS AND FUTURE WORK	38
5.1	Proposed Future Work	38
6	APPENDIX	40
6.1	Vacuum System Start-Up Procedure	40
6.2	Circular Polarisation of Light	40
	Bibliography	46

List of Figures

2.1	Energy level diagram of the hyperfine structure for the D ₂ line of ⁸⁷ Rb [1]. The splitting between the hyperfine levels and the allowed electric dipole transitions are shown. The approximate Landé g _F -factors for each level are also given, with the corresponding Zeeman splittings between adjacent magnetic sub-levels.	6
2.2	a) Profile of a typical atomic resonance, where ν _o is the resonant frequency of the atom. The influence of the Doppler effect when atoms are irradiated by a red detuned laser (frequency ν _L) is illustrated. b) Doppler effect used in laser cooling illustrated with the example of a single atom with velocity \vec{v} irradiated by two counter propagating red-detuned laser beams.	8
2.3	Maxwell gradient configured coils showing magnetic field lines. For the correct dimensions, L=2R	10
2.4	Illustration of the Zeeman shift of atomic energy levels and subsequent trapping force experienced by atoms impinged upon by counter-propagating circularly polarised laser beams in a linear magnetic field gradient.	11
2.5	Possible excitations involving σ ⁺ and σ ⁻ polarised light in the 5 ² S _{1/2} F = 2 → 5 ² P _{3/2} F' = 3 transition.	12
2.6	The trapping and re-pump transitions used in laser cooling of ⁸⁷ Rb	13
3.1	Saturated absorption spectroscopy setup	20
3.2	a) Schematic illustration of vacuum setup. b) Top view of 6-way cross piece and trapping cell.	22
3.3	A three dimensional schematic of the optical setup. All the beam steering mirrors are not shown. The optical isolator in front of the re-pump laser is not shown.	23
3.4	Illustration of the magnetic coils and spherical trapping cell. The coil area is represented by hatch lines. Current directions and dimensions of coils as indicated.	24
4.1	Turn on curve of re-pump laser showing a maximum power of 27.26 mW (at 110 mA) operated at 21.6°C. The threshold current is 32.77 mA. The slope efficiency is 0.35 mW.mA ⁻¹ . These values are obtained by applying linear fits to the data before and after the threshold. The fits are not shown.	26

4.2	Turn on curve of trapping laser (vortex system) showing a maximum power of 20.75 mW. We did not measure the operating temperature as this required linking the laser system to a computer and running diagnostic software. The threshold current is 31.83 mA. The slope efficiency is $0.48 \text{ mW}\cdot\text{mA}^{-1}$. These values are obtained by applying linear fits to the data before and after the threshold. The fits are not shown.	26
4.3	Illustration of optical setup for trapping ECDL showing trapping laser power only at various points. The trapping ECDL was operated at 74.8 mA and produced 20.4 mW of laser output. The optical isolator directly after the laser aperture is not shown. The re-pump laser (not shown) is included into the beam line at the second beam-splitter cube. The lenses used for beam expansion are also not shown.	28
4.4	Testing the effect of 45° mirror on the polarisation sense. From a) to b) the orientation of the fast axis of the quarter wave plates with respect to the horizontal x-axis was not changed.	30
4.5	Graph of simulated magnetic field strength versus position between coils along central axis courtesy of Ithemba labs [?]. The graph is anti-symmetric about the origin. Only the linear range from 0 mm to 5 mm is important. The gradient in this region is $16.4 \text{ G}\cdot\text{cm}^{-1}$	31
4.6	Graph of simulated magnetic field strength versus position between coils along transverse axis courtesy of Ithemba labs [?]. The graph is anti-symmetric about the origin. The linear range from 0 mm to 5 mm is of most interest. The gradient in this region is $7.7 \text{ G}\cdot\text{cm}^{-1}$	31
4.7	Graph of measured magnetic field strength versus position between coils along central axis. The zero of the x-axis is taken from an arbitrary point. Of most interest is the linear range from 13 mm to 23 mm. The gradient in this region is $17.2 \text{ G}\cdot\text{cm}^{-1}$	32
4.8	The Doppler broadened fine structure of Rubidium D2 line for ^{87}Rb and ^{85}Rb (above) and the hyperfine structure of the ^{87}Rb lines (both below).	33
4.9	Saturated absorption signal of the hyperfine structure of the $5S_{1/2}F = 2 \rightarrow 5P_{3/2}F' = X$ line for ^{87}Rb . The transition to $F' = 3$ is used for trapping. Peaks marked with an asterisk are crossover peaks.	34
4.10	Calibration plot for the $5S_{1/2}F = 2 \rightarrow 5P_{3/2}F' = X$ line. The relative frequency (MHz) of the peaks are plotted against their pixel position as given by the oscilloscope. The equation for the linear fit is shown.	34
4.11	Saturated absorption signal of the hyperfine structure of the $5S_{1/2}F = 1 \rightarrow 5P_{3/2}F' = X$ line for ^{87}Rb . The transition to $F' = 1$ or $F' = 2$ is used for trapping. Peaks marked with an asterisk are crossover peaks.	35
4.12	Calibration plot for the $5S_{1/2}F = 1 \rightarrow 5P_{3/2}F' = X$ line. The relative frequency (MHz) of the peaks are plotted against their pixel position as given by the oscilloscope. The equation for the linear fit is shown.	35
4.13	Fast Fourier transform of error signal of vortex laser in locking.	36

6.1	A sketch of the splitting of the energy levels by the Zeeman effect and the circularly polarised light required for the lower energy transition.	42
6.2	Illustration of the relation between angular momentum of light, its σ polarisation and its polarisation sense.	44
6.3	Illustration showing what happens to the polarisation sense during retro-reflection	45

List of Tables

2.1	Properties of rubidium [4][5][6]	5
-----	--	---

Chapter 1 - INTRODUCTION

1.1 Motivation

Traditionally when one would wish to spectroscopically investigate atoms or molecules in gaseous phase, the experiments would be conducted at room temperature. Consider the thermal-kinetic model of the energy of atoms:

$$\frac{1}{2}m\bar{v}^2 = \frac{3}{2}k_B T \quad (1.1)$$

where:

m	is the mass of the atom
\bar{v}	its mean velocity
k_B	the Boltzmann constant
T	the temperature in kelvin

Solving the above equation for the mean velocity of rubidium at room temperature shows that it is approximately 300 m.s^{-1} . This presents a problem as the speed of the atoms causes displacement and broadening of the spectral lines which makes accurate measurements more difficult to perform. In some cases refrigeration is used to lower the speed of the atoms, which is proportional to the square root of the temperature of the gas. Unfortunately in most traditional refrigeration techniques the atoms still have significant temperature with speeds in the order of 100 m.s^{-1} . Additionally the vapor pressure becomes so low that it is impractical to work with [1]. This has led to an increased interest in laser cooling of atoms.

Laser cooling has demonstrated cooling of groups of ^{87}Rb atoms to temperatures in the range of a few hundred μK , which corresponds to atomic speeds of a few millimeters per second. Other atoms are being investigated to determine if even lower temperatures can be achieved.

The discovery of laser cooling has enhanced our ability to do research on the physics of ultra-cold matter. This ultra-cold physics has led to the experimental realisation of a new phase of quantum matter first predicted by Einstein known as a Bose-Einstein condensate.

Ultra cold atoms also promise such future applications as quantum computers, atomic clocks for optical frequency standards and a general greater understanding into the nature of atoms.

As a result it is useful for anyone wanting to venture into the field of ultracold matter to have a solid grounding in the techniques used to produce ultracold atoms in laboratory conditions.

1.2 Aims

The aims of this M.Sc project are:

1. To study and investigate the physical principles of laser cooling and trapping of neutral atoms with specific focus on ^{87}Rb .
2. To develop an experimental setup for the trapping and cooling of neutral ^{87}Rb atoms.
3. To study the effect of the trapping parameters on the number and nature of trapped atoms in theory and practice.
4. To attain hands on experience of the physical requirements and allowable parameter ranges that lead to trapping and cooling of neutral atoms.

Chapter 2 - LITERATURE REVIEW AND PRINCIPLES OF TECHNIQUES EMPLOYED

2.1 Spectral Line Broadening

The width and shape of spectroscopic transitions will affect the ability to extract qualitative and quantitative information from a spectrum. The line shapes of spectroscopic transitions depend on the broadening mechanisms of the initial and final states, and include natural broadening, collisional broadening, power broadening, and Doppler broadening. Natural, collisional, and power broadening are homogeneous mechanisms and produce Lorentzian line shapes, and Doppler broadening is a form of inhomogeneous broadening and has a Gaussian line shape.

The excited state of an atom has an intrinsic lifetime due to radiative decay given by:

$$-\left(\frac{dN_j}{dt}\right) = N_j \sum_{(i<j)} A_{ji} \quad (2.1)$$

where N_j is the population in the excited state (j) and the A_{ji} 's are the Einstein spontaneous emission coefficients for all of the radiative transitions originating from level j . The negative sign arises because the rate decreases with time. Integrating this equation produces:

$$N_j(t) = N_j(0) \cdot e^{-\frac{t}{\tau_j}} \quad (2.2)$$

where $N_j(t)$ is the excited-state population at any time t , $N_j(0)$ is the initial excited-state population at $t = 0$, and τ_j is the radiative lifetime defined as:

$$\tau_j = \frac{1}{\sum_{(i<j)} A_{ji}} \quad (2.3)$$

Strong atomic transitions have A_{ji} 's of 10^8 to 10^9 s⁻¹, so lifetimes are 1 to 10 ns. The above expressions give only the radiative lifetime. Lifetimes can be shortened by collisions or stimulated emission.

The natural line width, ΔE (the intrinsic line width in the absence of external influences), of an energy level is determined by the lifetime Δt according to the Heisenberg uncertainty principle:

$$\Delta E \Delta t \cong \frac{h}{2\pi}$$

Thus the natural width of an energy level is:

$$\Delta E_j = \frac{h}{2\pi\tau_j}$$

or

$$\Delta E_j = \frac{h \sum_{(i<j)} A_{ji}}{2\pi}$$

Since $E = h\nu$

$$\Delta\nu = \frac{\sum_{(i<j)} A_{ji}}{2\pi} \quad (2.4)$$

where $\Delta\nu$ is the line width in frequency units considering a transition between an excited state and the ground state, the ground state has an essentially infinite lifetime, therefore the transition line width is governed by the width of the excited state.

The line shape of a transition with only natural broadening is a Lorentzian [2]. Collisional broadening occurs when collisions broaden spectroscopic line widths by shortening the lifetime of the excited states. The collisional broadening with regards to laser cooling is not significant due to the low pressures in the Rb cell and magneto optical trap [3]. Power broadening occurs by shortening the lifetime of the excited state due to stimulated emission. Power broadening with regards to laser cooling is not significant due to the low laser powers used. Doppler broadening is due to the distribution of atomic velocities (speed and direction), which each have a Doppler shift with respect to an observer. Doppler broadening is a prominent effect in laser cooling.

2.2 Properties of Rubidium

Various atomic elements may be used for the purpose of laser cooling and trapping of neutral atoms such as cesium [7], sodium [8] and rubidium, we shall be focusing on ^{87}Rb (27.85 % occurrence). Rubidium is a soft, silvery metal. It is one of the most active chemical elements. Rubidium is a member of the alkali family. The alkali family consists of elements in Group 1 (IA) of the periodic table. ^{87}Rb has 37 electrons, one being a valence electron. ^{87}Rb has two D line transitions named D_1 at 795 nm, and D_2 at 780 nm respectively.

The D_2 transition line is the one we are concerned with as it has a cycling transition that can be used for laser cooling. The Rubidium D_2 line is the transition from the ground state, $5S_{1/2}$, to the $5P_{3/2}$ state, namely the following transition:



The difference in energy between the $5S_{1/2}$ and the $5P_{3/2}$ levels is equivalent to a wavelength of 780 nm, or a frequency of $\sim 3 \times 10^{14}$ Hz. Both of these states can be further subdivided into hyperfine sub-levels denoted by F and F' in the ground and excited state respectively (see figure 2.1).

Property	Value
atomic number	37
atomic weight	85.4678
melting point	38.9 °C
boiling point	688 °C
specific gravity	1.53 at 20 °C
vapor pressure at 25°C	5.23×10^{-7} mbar
electron configuration	2-8-18-8-1 or [Kr]5s ¹
cooling transition	$5S_{1/2}F = 2 \rightarrow 5P_{3/2}F' = 3$
Nuclear spin	3/2
wavelength in vacuum	780.23 nm
Natural linewidth	5.9 MHz
Saturation intensity	1.6 mW.cm ⁻²
Recoil temperature	180 nK
Recoil velocity	0.59 cm.s ⁻¹

Table 2.1: Properties of rubidium [4][5][6]

The D line data for ⁸⁷Rb has been compiled by Steck [1] and is shown in figure 2.1.

2.2.1 Energy level splittings

The $5^2S_{1/2} \rightarrow 5^2P_{3/2}$ (D₂) and $5^2S_{1/2} \rightarrow 5^2P_{1/2}$ (D₁) transitions are the components of a fine-structure doublet [1], and each of these transitions additionally have hyperfine structure. The fine structure is a result of the coupling between the orbital angular momentum \mathbf{L} of the outer electron and its spin angular momentum \mathbf{S} . The total electron angular momentum is then given by

$$\mathbf{J} = \mathbf{L} + \mathbf{S} \quad (2.6)$$

and the corresponding quantum number \mathbf{J} must lie in the range

$$|L - S| \leq J \leq L + S$$

For the ground state in ⁸⁷Rb, $L = 0$ and $S = 1/2$, so $J = 1/2$; for the first excited state, $L = 1$ so $J = 1/2$ or $J = 3/2$. The energy of any particular level is shifted according to the value of J , so the $L = 0 \rightarrow L = 1$ (D line) transition is split into two components, the D₁ line ($5^2S_{1/2} \rightarrow 5^2P_{1/2}$) and the D₂ line ($5^2S_{1/2} \rightarrow 5^2P_{3/2}$). The meaning of the energy level labels is as follows: the first number is the principle quantum number of the outer electron, the superscript is the value given by $2S + 1$, the letter refers to L (i.e., $S \leftrightarrow L = 0$, $P \leftrightarrow L = 1$) and the subscript gives the value of J .

The hyperfine structure is a result of the coupling of \mathbf{J} with the total nuclear angular momentum \mathbf{I} . The total atomic angular momentum \mathbf{F} is then given by

$$\mathbf{F} = \mathbf{J} + \mathbf{I} \quad (2.7)$$

The magnitude of \mathbf{F} can have the values

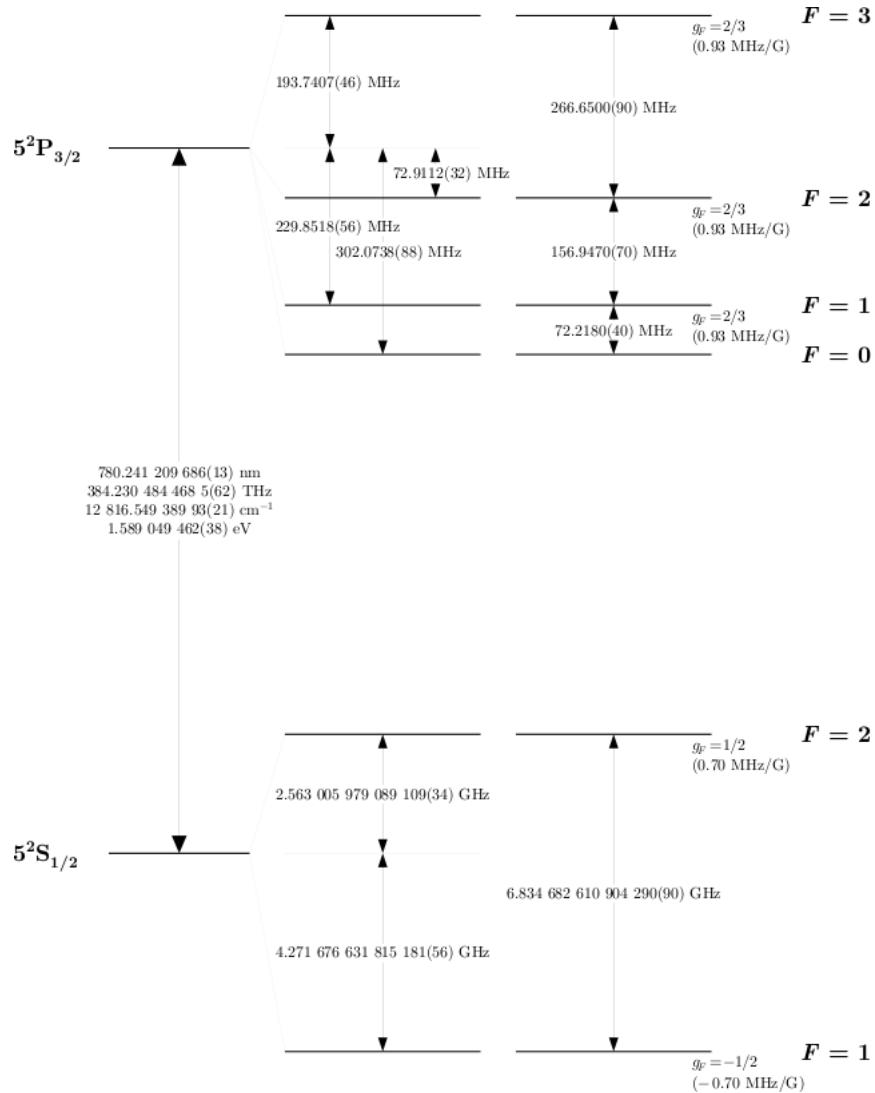


Figure 2.1: Energy level diagram of the hyperfine structure for the D_2 line of ^{87}Rb [1]. The splitting between the hyperfine levels and the allowed electric dipole transitions are shown. The approximate Landé g_F -factors for each level are also given, with the corresponding Zeeman splittings between adjacent magnetic sub-levels.

$$|J - I| \leq F \leq J + I$$

For the ^{87}Rb ground state, $J = 1/2$ and $I = 3/2$, so $F = 1$ or $F = 2$. For the excited state of the D_2 line, F can take any of the values 0, 1, 2, or 3. The atomic energy levels are shifted according to the value of F .

2.3 Principles of Laser Cooling and Magneto Optical Trapping

Laser cooling and trapping relies on the nature of the interaction between laser light and atoms.

Essentially, the absorption and emission of light by an atom has the ability to change the momentum of the atom. Absorption of light leads to the transfer of momentum from the photon to the atom and an increase in the internal energy of the atom. If the atom decays by spontaneous emission (as is the case in fluorescence), the recoil associated with the decay (production of a photon) is in a random direction. Thus the average over many emission events results in a zero net effect on the atomic momentum. It is easy to see that a laser beam would have a resultant force on an atom since when photons are being absorbed, all the momentum is in one direction. Metcalf gives a quantum mechanical treatment of the absorption and emission mechanism [9].

The laser control of atoms and molecules usually uses the process of resonant absorption and emission of photons. Resonant absorption and emission of photons by atoms/molecules is considered a special case of elastic scattering of photons.

In elastic scattering the atom and the photon being scattered exchange only their momenta without a change of the internal energy of the atom. In such scattering, the scattered photon changes the direction of its momentum, and so does the scattering particle.

As the frequency of the scattered photon approaches a resonance frequency, the scattering cross section increases as illustrated in figure 2.2. At the resonant frequency it coincides with the maximum resonant absorption cross section and the processes of resonant absorption and subsequent spontaneous decay become inseparable from the resonant scattering process [10]. The frequency dependence of the cross section has a Lorentzian profile.

For the purposes of this thesis, we shall model the effect that light has on an atom with scattering theory. The primary decelerating force in the laser cooling of atoms is the transfer of momentum from photons scattering off an atom. While the effect per photon is quite small (the change in the velocity imparted is in the order of 1cm/s) [11], a large number of photons can be scattered off the atom per second. If the incident photons' momenta have the same direction, and since the direction in which the photons are subsequently scattered are random, the atom will experience a net impulse in the direction of the incident photons' momentum due to the momentum transfer of the elastic scattering. The photon bombardment is constructed such that the atoms in a sample are slowed to a near zero velocity and thus cooled. This is made possible by using the Doppler effect making the photon scattering dependent

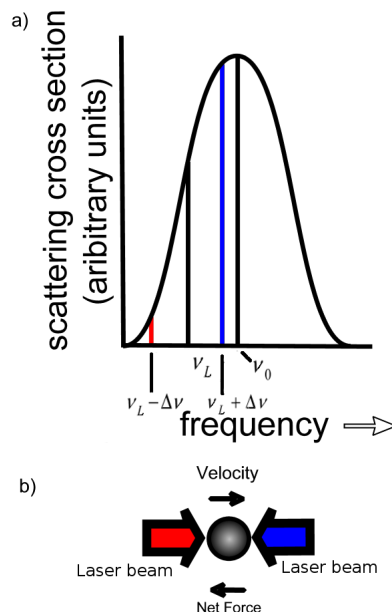


Figure 2.2: a) Profile of a typical atomic resonance, where ν_0 is the resonant frequency of the atom. The influence of the Doppler effect when atoms are irradiated by a red detuned laser (frequency ν_L) is illustrated. b) Doppler effect used in laser cooling illustrated with the example of a single atom with velocity \vec{v} irradiated by two counter propagating red-detuned laser beams.

on the relative velocity of the atom. The Doppler shift of an incident light field of frequency ν_L due to motion of the atom is

$$\Delta\nu_d = \frac{v_{atom}}{c} \nu_L \quad (2.8)$$

for small atomic velocities relative to c .

Firstly the laser frequency ν_L is red detuned from the resonance peak of the absorption line used for laser cooling as illustrated in figure 2.2.

In figure 2.2, if the atom has a velocity to the right, it will see the beam propagating to the left as Doppler shifted to a higher frequency and thus encounter a higher photon scattering rate from this beam and therefore a larger impulse to the left. Conversely the atom will see the beam propagating to the right as having a lower frequency and will thus encounter a lower photon scattering rate from this beam and therefore smaller impulse to the right. The combined effect serves to cause a net force opposite to the atom's direction of motion. This technique is commonly referred to as Doppler laser cooling.

The recoil velocity v_r is the change in the ^{87}Rb atomic velocity when absorbing or emitting a resonant photon, and is given by

$$v_r = \frac{\hbar k_L}{m} \quad (2.9)$$

where k_L is the wave-number and m is the mass of the atom.

The recoil energy $\hbar\omega_r$ is defined as the kinetic energy of an atom moving with velocity $v = v_r$, which is

$$\hbar\omega_r = \frac{\hbar^2 k_L^2}{2m} \quad (2.10)$$

The recoil temperature is the temperature corresponding to an ensemble with a one-dimensional rms momentum of one photon recoil $\hbar k_L$

$$T_r = \frac{\hbar^2 k_L^2}{mk_B} \quad (2.11)$$

The Doppler temperature [1],

$$T_D = \frac{\hbar\Gamma}{2k_B} \quad (2.12)$$

(where Γ is the spontaneous decay rate or Einstein A coefficient which is also the natural (homogenous) line width of the emitted radiation) is the lowest temperature to which one expects to be able to cool two-level atoms in optical molasses, due to a balance of Doppler cooling and recoil heating. In Zeeman-degenerate atoms, sub-Doppler cooling permits temperatures below this limit.

If counter propagating laser beams are directed at the atom along three mutually orthogonal axes, (along the standard x, y, and z axes in Cartesian co-ordinates) then the majority of the forces will cancel out and that which remains is the velocity dependent force which provides a strong dampening of atomic motion. This setup of laser beams is known as an optical molasses. Three pairs of counter propagating beams are sufficient to cool an atom with any direction of motion since any velocity can be broken up into vectors parallel to the axes of the molasses.

An optical molasses by itself will not spatially trap atoms since there is no position dependent force. A position dependent force can be achieved by meeting the two requirements of:

1. applying a three dimensional magnetic field gradient across the center of the optical molasses, and
2. introducing the appropriate circular polarisation of the counter-propagating laser beam pairs with the aid of quarter wave plates.

Two magnetic field coils with oppositely directed currents and spaced a distance equal to their diameter apart as shown in figure 2.3 create a magnetic field gradient which is zero in the center and changes linearly along the axes. The value of the magnetic field at a point along the central axis between the two coils may be calculated with the aid of the following formula:

$$B(x) = \frac{\mu_0 n I R^2}{2(R^2 + x^2)^{\frac{3}{2}}} - \frac{\mu_0 n I R^2}{2(R^2 + (L - x)^2)^{\frac{3}{2}}} \quad (2.13)$$

where:

B is the magnetic field in Gauss

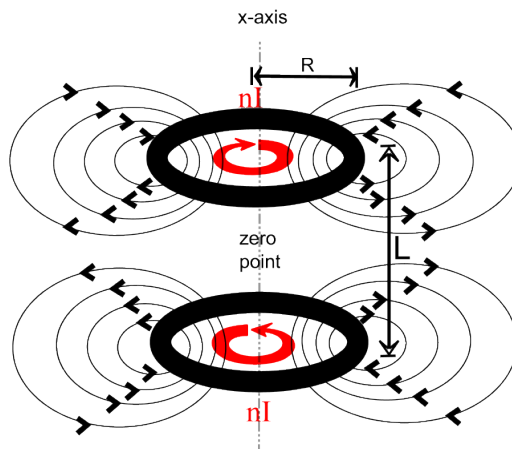


Figure 2.3: Maxwell gradient configured coils showing magnetic field lines. For the correct dimensions, $L=2R$

- μ_0 is the permeability of free space
- n is the number of turns on the coil
- I is the current in ampere through the coil
- R is the radius of the coil
- L is the separation distance between the two coils
- x is the position at which the magnetic field is to be determined

It can be shown that the magnetic field gradients along the non-coaxial axes are also linear and have a zero point at the center of the two coils.

As the laser light leaves the external cavity diode lasers (ECDLs) it is linearly polarised. Linearly polarized light can be converted to circularly polarized light by slowing one component of the field. This is achieved by using a birefringent material of the appropriate thickness. For our purposes we use commercially available quarter wave plates (rated for 780 nm light) that retard one component of the electromagnetic wave by a quarter of its wavelength. The appropriate circular polarisation of the counter-propagating beam is achieved by passing the original beam through a second quarter wave plate (after passing through the center of the molasses) and then retro-reflecting the beam causing it to go through the same quarter wave plate once more. After two passes through the quarter wave plate and reflection off a metal mirror, the beam has undergone a total of 360 degrees phase change of one of its components, which results in the correct circular polarisation sense of the returning beam (This is discussed in greater depth in the appendix 6.2).

In figure 2.4, three atoms are depicted at different positions in a magnetic field gradient and subjected to counter-propagating, oppositely circularly polarised laser beams. When a magnetic field is applied over an atom, a Zeeman shift of the atomic energy levels occurs, the shift in energy levels affects the rate at which atoms at a particular spatial position scatter photons from the laser beams. The laser light from the left-hand side is σ^- polarised and the light from the right-hand side is σ^+ polarised. Due to the rule of conservation of angular momentum, the σ^- polarised light may only cause a transition during which the change in magnetic spin quantum number is $\Delta m = -1$. Similarly the σ^+ polarised light may only cause a transition in which the change is $\Delta m = +1$.

If an atom were to find itself to the left of the origin (position 1 in fig 2.4) where the magnetic field is parallel to the chosen z-axis, it would encounter a Zeeman splitting such that the $m_f = -1$ transition is tuned closer to resonance and thus the scattering rate of the σ^- photons increases. Conversely the $m_f = +1$ transition would be tuned further from resonance and thus decreasing the scattering rate of the σ^+ photons. The combined result is an impulse towards the right. Similarly, if an atom were to find itself on the right-hand side of the origin (position 3) it would encounter an impulse towards the left and if it were at the origin (position 2) it would experience no net impulse. This results in the atoms being trapped at and around the origin. This configuration of an optical molasses of polarized light and gradient magnetic field used to cool and subsequently spatially trap atoms is named a magneto-optical trap (MOT).

Of course there are more possible transitions than the two examples given above due to the different m_f values available in the ground and excited state of the $5^2S_{1/2}F = 2 \rightarrow 5^2P_{3/2}F' = 3$ transition. All the possibilities resulting from σ^+ and σ^- polarised light are shown in figure 2.5.

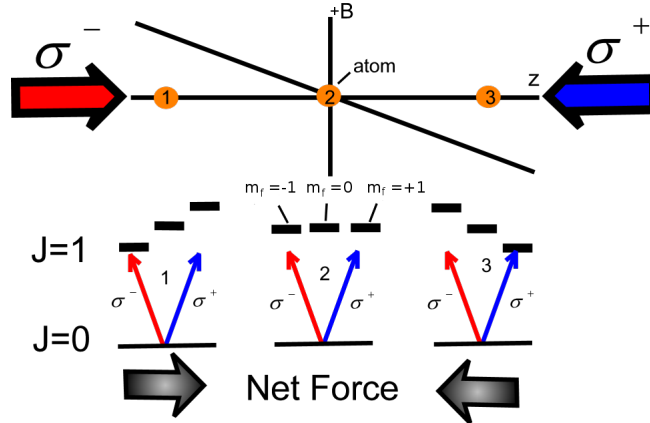


Figure 2.4: Illustration of the Zeeman shift of atomic energy levels and subsequent trapping force experienced by atoms impinged upon by counter-propagating circularly polarised laser beams in a linear magnetic field gradient.

The cooling and trapping is done by one laser which is tuned to the lower frequency side of the $5S_{1/2}F = 2 \rightarrow 5P_{3/2}F' = 3$ transition of ^{87}Rb . This

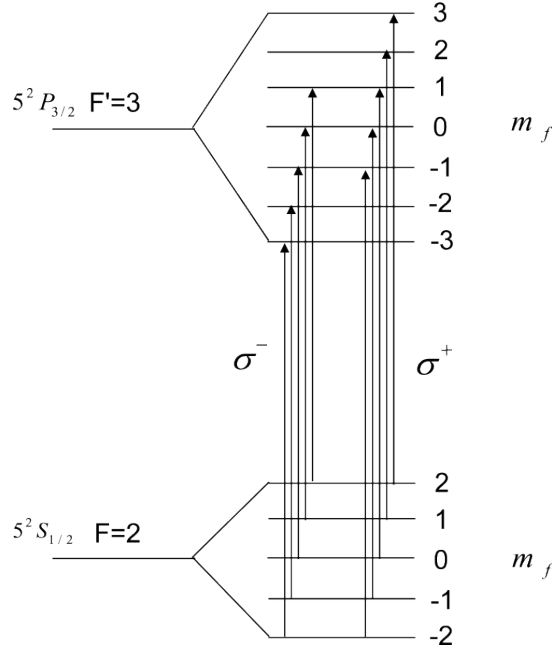


Figure 2.5: Possible excitations involving σ^+ and σ^- polarised light in the $5^2S_{1/2}F = 2 \rightarrow 5^2P_{3/2}F' = 3$ transition.

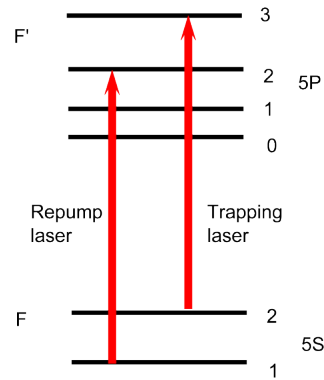
excitation is possible with a tunable laser operating at approximately 780 nm. About one in every thousand of the atoms excited to the $5P_{3/2}F' = 3$ state will decay back to the $5S_{1/2}F = 1$ state. The trapping laser cannot excite atoms out of this state and if they are allowed to remain in this ground state, the trapping of atoms will no longer be possible. This decay to a different ground state and subsequent drop in the number of atoms available to be excited from the former ground state is referred to as optical pumping.

Thus it is necessary to have an additional laser operating at 780 nm (but slightly different to the trapping laser) to excite atoms from the $5S_{1/2}F = 1$ state to the $5P_{3/2}F' = 2$ or $F' = 1$ state where they may decay back to the $5S_{1/2}F = 2$ state and are once again able to interact with the trapping laser beams. This second laser is referred to as the re-pump or hyperfine pumping laser.

2.4 Parameters Influencing the Number of Trapped Atoms

In a typical Rb vapor cell trap the Rb atoms in the low energy tail ($V < V_{max} \simeq 20m.s^{-1}$) of the Maxwell-Boltzmann distribution are captured in the trap. If the trap is turned on at $t = 0$, the number N of atoms in the trap will increase with the same functional form as a charging capacitor [11].

$$N(t) = N_0 \left(1 - e^{-\frac{t}{\tau}}\right) \quad (2.14)$$


 Figure 2.6: The trapping and re-pump transitions used in laser cooling of ^{87}Rb

Where τ is the time constant for the trap to fill to its steady state value N_0 and is also the average time an atom will remain in the trap before it is knocked out by a collision. This time is just the inverse of the loss rate from the trap due to collisions. Under certain conditions, collisions between trapped atoms can be important, but for conditions that are usually encountered, the loss rate will be dominated by the collisions with the room temperature background gas. These background atoms and molecules have more than enough energy to knock atoms out of the trap. The time constant τ can be expressed in terms of the cross sections σ , densities n , and velocities of Rb and non-Rb components as:

$$\frac{1}{\tau} = n_{\text{Rb}}\sigma_{\text{Rb}}V_{\text{Rb}} + n_{\text{non}}\sigma_{\text{non}}V_{\text{non}} \quad (2.15)$$

The steady-state number of trapped atoms is that value for which the capture and loss rates of the trap are equal. The capture rate is simply given by the number of atoms which enter the trap volume (as defined by the overlap of the laser beams) with speeds less than V_{max} . This is proportional to the Rb density, $(V_{\text{max}})^4$ and the surface area A of the trap. When the background vapor is predominantly Rb, the loss and capture rates are both proportional to Rb pressure. In this case N_0 is given by:

$$N_0 = \left(\frac{0.1A}{\sigma_{Rb}} \right) \left(\frac{V_{max}}{V_{avg}} \right)^4 \quad (2.16)$$

Where $V_{avg} = \left(\frac{3k_B T}{m} \right)^{\frac{1}{2}}$ (derived from equation 1.1), the average velocity of the Rb atoms in the vapor. If the loss rate due to collisions with non-Rb background gas is significant, Eq. 2.16 must be multiplied by the factor

$$\frac{n_{Rb}\sigma_{Rb}V_{avg}}{n_{Rb}\sigma_{Rb}V_{avg} + n_{non}\sigma_{non}V_{non}} \quad (2.17)$$

The densities are proportional to the respective partial pressures. Finally, if the loss rate is dominated by collisions with non-Rb background gas, the number of atoms in the trap will be proportional to the Rb pressure divided by the non-Rb pressure, but τ will be independent of the Rb pressure.

A magneto optical vapor trap is a highly over damped system; hence damping effects are more important for determining trap performance than the trapping force is. Because it is highly over damped, the critical quantity V_{max} is determined almost entirely by the Doppler slowing which provides the damping.

The cross sections for collisional loss are only very weakly dependent on the depth of the trap, and therefore the trap lifetime is usually quite insensitive to everything except background pressure. As a result of these two features, the number of atoms in the trap is very sensitive to laser beam diameter, power, and frequency, all of which affect the Doppler cooling and hence V_{max} . However, the number of trapped atoms is insensitive to factors which primarily affect the trapping force but not the damping, such as the magnetic field and the alignment and polarisations of the molasses beams. Obviously, if the trapping potential is changed enough so that there is no potential minimum (for example if the zero point of the magnetic field is no longer within the overlap of the molasses beams), there will be no trapped atoms. However, as long as the damping force remains the same, almost any potential minimum will have approximately the same number of atoms and trap lifetime.

We may determine the number of atoms in the MOT experimentally by imaging the fluorescence induced by the trapping and re-pump lasers onto a photo diode. The line of sight from the collection lens through the glass wall, to the center of the MOT cloud, and onto the far glass wall, should not include any section of the glass wall that is illuminated by a trapping beam, as this results in too much scattered laser light hitting the photo diode. The photo diode is shielded by a tube of black paper so that it can “see” only the collection lens. Collecting some scattered light is unavoidable. Most of this comes from stray light scattering from imperfections in the glass cell; at low vapor pressures (below 10^{-4} mbar), essentially none of the scattered light comes from the background Rubidium vapor in the cell. In any case we subtract out the background scattered light level, which we establish by turning off the MOT magnetic coils.

The number of atoms in the MOT is given by

$$N = \frac{4\pi I}{\sigma\rho\varepsilon_p R(0.96)^k} \quad (2.18)$$

where:

I	is the photo diode current
σ ,	the solid angle subtended by the collection lens
ρ ,	the responsivity of the photo diode
ε_p ,	the energy of a single photon
k ,	the number of uncoated glass surfaces between the vapor cloud and the photodetector
R ,	the photon scattering rate in photons.s ⁻¹ .atom ⁻¹ is given by

$$R = \frac{\frac{I_0}{I_s} \pi \Gamma}{1 + \frac{I_0}{I_s} + 4 \left(\frac{\Delta}{\Gamma}\right)^2} \quad (2.19)$$

where:

I_0	is the total intensity of the six beams impinging on the atoms,
I_s ,	the saturation intensity, which is 4.1 mW.cm ⁻² for random polarization for Rb.
Γ ,	the natural line width of 5.9 MHz for Rb,
Δ ,	the detuning from resonance.

According to the Lewandowski group, using the I_s appropriate for random polarization gives the most accurate number of atoms in a MOT [5].

To determine the temperature of the trapped atoms, most groups employ a time of flight technique. In this technique, an established trap is turned off and the atoms allowed to diffuse. Transient absorption is performed on the diffusing cloud to determine it's rate of expansion and thereby it's temperature. Silva et al. [12] have studied this in depth and demonstrated an improved technique.

2.5 Literature on Magneto Optical Trap Setups.

For an overview of the history of laser cooling one may read the article by W.D. Phillips [13]. For the most part, the paper by Wieman et al. [11] is used as a basis for this work.

Lewandowski et al. [5] describe a more optimised MOT system capable of producing a Bose-Einstein condensate in detail.

2.5.1 External cavity diode lasers

The Wieman group made use of two diode lasers which produced narrow band tunable light [14]. They state that 5mW of laser power per laser is sufficient for laser cooling.

The Lewandowski group [5] make use of three lasers, each at different wavelengths, in their setup for a Bose-Einstein condensate. Two lasers are used to perform trapping in the normal way and a third laser is used to image the condensate that forms in their trap. For their MOT's trapping beams they

make use of a commercial ECDL which is amplified by a single pass through a tapered amplifier chip, in a master-oscillator power-amplifier (MOPA) configuration. This system will nominally produce 500 mW of power at 780 nm (this large power is due to wanting to trap a large amount of atoms with which to obtain a BEC). The probe beam and the MOT's hyperfine re-pump beam are supplied by two separate ECDLs, which each produce approximately 8 mW.

The Lewandowski group also stresses that vibration isolation is important when operating ECDLs (they use commercial New Focus Vortex lasers). Vibration can cause frequency noise at a level that the feedback may not be able to suppress fully. They mount their trapping and hyperfine re-pump lasers on a piece of 6 mm thick sorbathane sheeting to reduce the effect of vibrations from the table, which is additionally isolated from the floor by air bladders in the table legs. They also mount their mechanical shutters on sorbathane, so that vibrations induced by the solenoids when they open or close are not transmitted to the optical table.

Another concern with the operation ECDLs is electrical ground loops, which can cause noise on the laser. To limit this noise all of the electronics used for the laser and frequency locking should use the same electrical outlet.

2.5.2 Saturated absorption spectroscopy and frequency locking

Both groups' lasers are locked to atomic transitions in Rb^{87} using saturated absorption spectroscopy in the same method described later in this text (see section 3.3).

The Wieman group locks each laser to the red side of the peak of an atomic transition [14].

The Lewandowski group locks each laser to the peak of an atomic transition. They state that the frequency location of the peak of the transition is relatively insensitive to intensity and broadening effects, which would change the locking set point if the laser were locked instead to the side of the line as is the case with the Wieman group. Unfortunately a servo can only lock to a region where there is a slope of the line to use as feedback. The standard solution to this problem is to generate a derivative of the saturated absorption signal. They modulate the frequency of the laser, by modulating either the electrical current driving the laser or the radio frequency driving an acousto-optic modulator (AOM). The modulation has a depth of 5 MHz at a rate of 50 kHz, which is slow enough for the AOMs to respond and fast enough to be above the bandwidth of the servo. The signal from the saturated absorption spectrometer is routed to a homemade lock-in detector, which gives the derivative of the original transition lines. The derivative changes sign at the absorption peak, and thus when compared to a zero-volt reference, is a convenient error signal for their servo.

Their setup allows them to lock the laser to the peak of the $F = 2 \rightarrow F' = 2$, $F = 2 \rightarrow F' = 3$ crossover saturation line and have the trapping light red detuned by several natural line widths from the cooling transition. Their re-pump laser is locked directly to the re-pump transition.

2.5.3 Vacuum system and atomic rubidium source

The Wieman group's vacuum system consists of a roughing pump, turbo molecular pump and a 8 l/s ion pump. Their glass trapping cell is an epoxied square based prism construction. They suggest the alternatives of having a glassblower make a six-sided glass cross with six windows on the tubes of the cross and a glass to metal seal that allows the glass cell to be attached to the system. Another alternative is to buy a commercial six-way cube with conflat-type flanges and six view ports which are windows mounted on stainless steel conflat flanges. This option is however expensive and limits the viewing and optical access.

The Lewandowski group's vacuum system is comprised of a high vacuum MOT cell (10^{-8} Torr) and an UHV (10^{-11} Torr) science cell. Three vacuum pumps are used in the system, but only one of them is used on a continual basis. The turbo pump, connected to the system by an all-metal valve, is used only during initial pump down and bake out. The Ti-sublimation pump is turned on only every couple of years to remove extra Rb or H from the system. The workhorse pump is the 40 l/s ion pump, which pumps continuously on the system during normal operations.

The differential pressure between the two chambers is maintained by placing a small aperture between the two chambers to reduce the conductance. An aperture diameter of 5 mm was chosen because it allows most of the atoms in the quadrupole trap through when the cloud has a temperature of 200 mK and yet limits the conductance enough to have an adequate pressure in the UHV region.

The science and MOT cells are cylindrical glass cells attached to glass-to-metal seals. Quartz cells are more permeable than Pyrex to atmospheric helium and should be avoided in UHV regions of the system.

In both groups Rb getters are used as a source. The getter assembly consists of a current feed-through and one or two Rb dispensers (getters). The Rb getters are a controllable source of Rb vapor. A getter is a small foil container of a Rb salt, which releases Rb when a moderate current of 2 to 6 A is run through the device. Special care must be taken with the getters to ensure they will produce clean Rb vapor. The getter material can easily absorb water, so they store them under vacuum with desiccant and flow dry gas during the glass fusing process. A proposed mode of operation is to turn on the getters at 3.5 A for 10 minutes to supply the MOT cell with a day's worth of Rb, and then to allow 10 to 20 min for the contaminants to pump out of the system before taking data. Getters that are less contaminated can be run continuously throughout the day at a lower current. Because of the way in which rubidium vapor coats the inside of the vacuum system, its pumping speed is extremely low, so the pressure reading for instance on the ion-pump controller current will have little to do with the rubidium pressure in the MOT cell. Rubidium pressure can be determined locally by looking at absorption on a beam through the cell, but pressures are best understood and measured in terms of inverse lifetimes of trapped atoms. One would like the lifetime in the MOT cell to be about 5 to 10 seconds, and in the science cell to be in excess of 100 seconds. One is aiming to have a partial pressure of Rubidium of something less than 10^{-9} Torr and a partial pressure of all impurity gases lower than the Rubidium pressure by at least a factor of two.

2.5.4 Optical setup for an optical molasses

The Wieman group makes use of three orthogonal laser beam paths that are formed from splitting the beam from the trapping laser and are retro-reflected to form their optical molasses.

The Wieman group states that the operation of the trap is remarkably insensitive to the relative amounts of power in each of the beams.

For the hyperfine re-pump laser the Wieman group states that the only requirement is that the laser light cover the overlap region of the optical molasses. This means that a single beam (with expansion optics) is sufficient to provide re-pump light for the trap to function. They state that the trap is insensitive to nearly everything concerning the hyperfine re-pump light, including its polarisation.

The Lewandowski group makes use of a total of 5 polarising beam-splitter cubes with half-wave plates before each to split their trapping beam into six separate beams which are all directed into the trapping cell from the six sides. Although they do not make use of retro-reflecting mirrors, their alignment is such that the molasses beams are counter propagating. This allows them to independently control the power in each beam by adjusting the rotation of the half wave plate before the appropriate beam splitter cube. The number of trapped atoms increases rapidly with the size of the beams. The Wieman group suggests a beam diameter of 1.5 cm as smaller beams have increased alignment sensitivity whereas with larger beams they become difficult to fit onto 2.5 cm optics as well as more difficult to view due to decreased intensity.

2.5.5 Magnetic field coils

Two symmetric magnetic field coils with oppositely directed currents will create a magnetic field which is zero in the center and changes linearly along the x, y and z axes.

The Wieman group simply glues or tapes two coils to the sides of their trapping cell. They use two freestanding coils of 1.3 cm diameter with 25 turns each of 5 mm diameter magnet wire. When mounted the coils have a separation of 3.3 cm. They send 2-3A of current through them to produce the desired gradients.

The Lewandowski group's MOT coils which also serve as the quadrupole trap coils, are each made of 24 turns of square hollow copper tubing coated with Kapton. The wire has a square cross-section of 4.15 mm on a side with a round 2.5 mm diameter hole in the center. The coils are cooled by running water through the center region of the wire. The wire is wound onto a phenolic spool and secured with epoxy. Phenolic was chosen as the spool material because it will not support eddy currents when the current is abruptly changed in the coils. The inner diameter of the coils is 5 cm, and their centers are separated axially by 10 cm. The coil configuration produces a magnetic field gradient of $1 \text{ Gauss.cm}^{-1}.\text{A}^{-1}$ along the axis of the coils.

Chapter 3 - EXPERIMENTAL SETUP

3.1 Overview

For the establishment of a magneto optical trap, the following components are required:

1. Two laser light sources (complete with various control electronics), one for trapping and one for optical re-pump, which are frequency tunable around the resonance frequency of the atom to be trapped.
2. Two setups to perform saturated absorption spectroscopy in rubidium vapor sample cells so that the lasers may be frequency locked to the appropriate absorption lines of the atom.
3. Side-lock servo electronics with which to lock the laser's frequency.
4. A vacuum system capable of evacuating a transparent glass trapping cell to pressures in the vicinity of 5×10^{-7} mbar.
5. A source of atomic rubidium vapor by which the vapor may be introduced into the vacuum system and trapping cell.
6. Appropriate optics to set up an optical molasses and re-pump beam.
7. Magnetic field coils with which to create a gradient magnetic field in the order of 10 Gauss.cm^{-1} in the trapping cell.

3.2 External Cavity Diode Lasers

For the trapping laser a commercially available frequency tunable external cavity diode laser (ECDL) (New Focus Vortex 6013) is used [15]. It is capable of 20 mW of continuous wave laser output at 780 nm. For the re-pump an in-house built ECDL (using laser diode HL7851G from Thorlabs) is used [16].

For the home built laser, separate control equipment was also built to control the diode temperature, the current through the diode and the orientation of the grating that forms the end of the external cavity. The home built ECDL is constructed in a Littrow configuration [16].

The Vortex laser has one integrated control unit controlling the laser diode current, the temperature and the base voltage delivered to the piezo responsible for micro positioning of the grating. The Vortex laser has a Littrow-Metcalf configuration. In both lasers an optical element in the external cavity is mounted on a piezo. This facilitates its micro positioning (or fine tuning of its orientation) to achieve tuning and scanning of the output frequency under

electronic control. There are three modes: manual tuning, scanning of laser frequency back and forth over a user defined frequency range and locking of the laser frequency with the aid of saturated absorption spectroscopy setups and side-lock servo electronics to the desired hyperfine lines of ^{87}Rb .

3.3 Saturated Absorption Spectroscopy and Frequency Locking

The setup for saturated absorption spectroscopy (SAS) is illustrated in figure 3.1. At the output of each laser, a 20 mm thick perspex slab is inserted which samples off approximately 6% of the laser beam's total power. The reason for using such a thick beam sampler is that the two reflections from a thick slab are clearly separated in space and only one can be used for SAS without interference of the second reflected beam. This sample beam is again passed through a 10 mm thick glass slab which samples off two probe beams (here both reflections are used). The remaining transmitted beam is used as the pump beam.

These two probe beams are directed through a rubidium vapor cell where they undergo absorption by the atomic rubidium vapor and are then directed into two photo detectors connected to a PID (product integration differentiation) amplifier which processes the signals by taking the negative of one and then summing the result together so the output signal is the difference between the two signals. The output is balanced by adjusting the gain of the two signals in the PID unit so that, in the absence of the pump beam, the two absorption signals cancel each other out. The transmitted pump beam is directed to counter propagate and spatially overlap one of the probe beams inside the vapor cell.

The saturated absorption spectroscopy signal serves as an input signal for the side-lock servo electronics that are used to frequency lock the lasers. The operation of the side-lock servo and the technique of frequency locking has been described previously in the masters thesis by G.N. Botha [3].

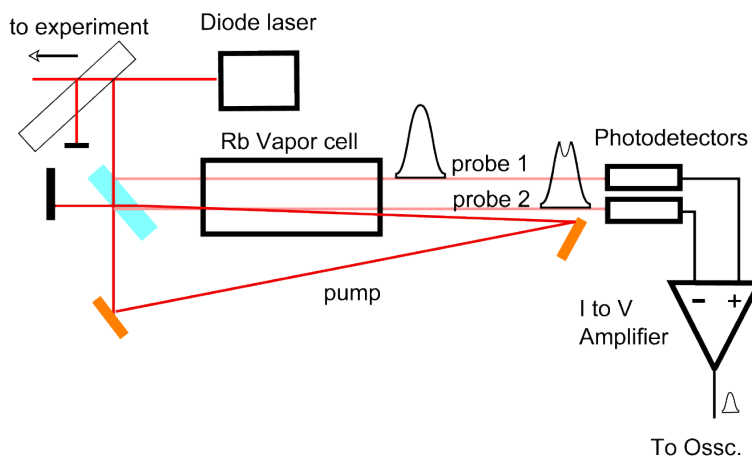


Figure 3.1: Saturated absorption spectroscopy setup

3.4 Vacuum System and Rubidium Source

A vacuum system capable of evacuating a glass trapping cell to pressures in the region of 10^{-7} mbar is used as illustrated in figure 3.2. It consists of a roughing pump which is connected via flexible metal tubing with KF-flanges, containing o-ring seals, to a rubber seal angle valve which is in turn connected to a turbo-molecular pump. The turbo pump is connected directly to an electronically controlled and pneumatically operated gate valve which closes if the electrical power to it's controller is switched off. Above the gate valve is a conversion pipe from a KF flange to a 16CF metal seal flange. This conversion pipe also accommodates a connection to a vacuum guage. Above the conversion pipe is a metal seal angle valve that can be used to isolate the high vacuum system (metal sealed) from the turbo pump. The angle valve is connected to a 6-way cross piece.

Attached on each of the five remaining flanges of the 6-way cross piece are:

1. A 16CF to 40CF conversion flange onto which the glass trapping cell is glued with vacuum epoxy.
2. An extension pipe inside which the rubidium getter, attached to an electrical feed-through, is housed.
3. A window attached directly opposite the trapping cell.
4. A second extension pipe connecting to an ion-pump.
5. A blank flange.

Once sufficient vacuum level is achieved by running the various pumps (see appendix 6.1 for pump down procedure), the atomic rubidium vapor is introduced into the trapping cell by applying an electrical current through the getter. (SAES Getters, part nr. 5G0125, model RB/NF/3.4/12 FT10+10). The amount of vapor present in the cell can be controlled by adjusting the current through the getter. A typical current applied to the getter is 9 Ampere.

Two interchangeable trapping cells were designed. The prism trapping cell consists of four rectangular glass slides measuring 40 mm by 27 mm by 3 mm and one 30 mm square piece at 3 mm thickness. These are glued into a prism with vacuum epoxy. The second cell is 30 mm diameter spherical with a 23 mm diameter cylindrical branch and constructed by a glass blower into one piece. These cells are glued onto a 16CF to 40CF conversion flange with vacuum epoxy. An important advantage to using a spherical trapping cell is that the interference fringes on the trapping beams have higher spatial frequency and are spaced less regularly than with a square cell. These relatively fine structure intensity fringes have little effect on the trapped atoms but make viewing of a clear image of the MOT with the aid of a camera easier. MOT alignment with a square cell can be more difficult because it is important to place the minimum of the broad intensity fringes away from the center of the trap. This type of alignment requires more frequent adjustments [5].

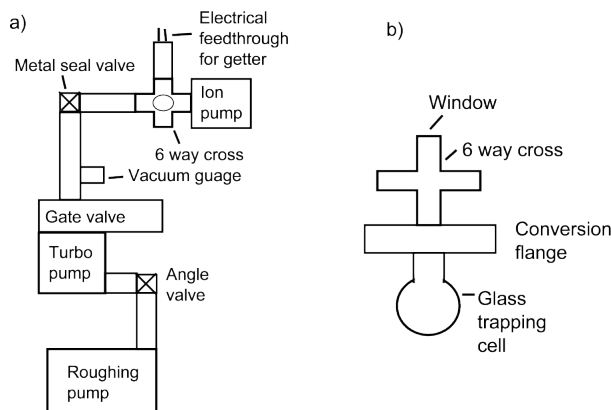


Figure 3.2: a) Schematic illustration of vacuum setup. b) Top view of 6-way cross piece and trapping cell.

3.5 Optical Setup for an Optical Molasses

The optical setup is illustrated in figure 3.3. The trapping and re-pump laser beams first pass through an optical isolator which is in place to prevent accidental feedback to the laser which may cause the laser output to be less stable. The beam passes through a beam sampler where approximately 4% of its intensity is sampled off to the saturated absorption spectroscopy setup. The beam then passes through a diverging and converging lens respectively so that it is expanded to a 1.5 cm diameter beam. The beam may be cleaned up with the aid of an iris which is located after the expansion lenses (or alternatively focused through a pinhole during the expansion process).

The beam is brought to the working height (12 cm above the optical table) and aligned through a half wave plate (to adjust the percentage power in the beams), a Glan-Taylor prism and beam splitter to split the main beam into three beams of similar intensity.

These beams are aligned through the trapping cell and onto retro-reflecting mirrors on the three mutually orthogonal horizontal and vertical Cartesian axes such that all three beams and their retro-reflections overlap in the approximate center of the trapping cell to form the optical molasses. Two quarter wave plates are introduced into each beam, one on each side of the trapping cell to provide oppositely directed circular polarisation to the laser light in the counter-propagating beams. Although not depicted as such in figure 3.3, the vertical molasses beam in the setup first goes through a quarter wave plate and then onto a 45° mirror where it is then directed into the trapping cell. This reflection affects the polarisation sense of the light by changing it from counter-clockwise to clockwise or vice versa. Experiments were done to confirm this effect and care must be taken to account for this change when setting the orientation of the quarter wave plates.

The re-pump beam is combined co-linearly with the trapping laser beam at the second Glan-Taylor prism after going through a half wave plate to be able to adjust the total power sent into the beam line. It is split once more with the trapping beam and is thus present in 2 of the 3 molasses beam axes.

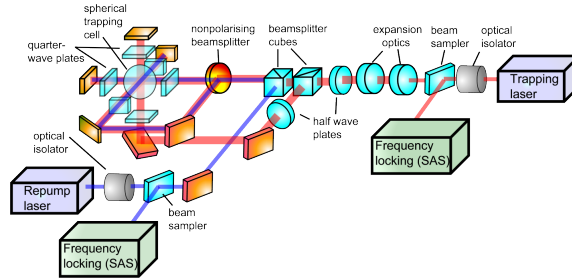


Figure 3.3: A three dimensional schematic of the optical setup. All the beam steering mirrors are not shown. The optical isolator in front of the re-pump laser is not shown.

3.6 Magnetic Field Coils

The magnetic field coils and the approximate magnetic field they produce are illustrated in figure 2.3. Using formula 2.13 it was calculated that we require 200 turns at 500 mA with the dimensions shown in figure 3.4 to achieve a gradient of approximately 15 G.cm^{-1} . A custom designed magnetic coil mount was constructed to bolt onto the conversion flange to which the trapping cell is attached. It mounts two coils of 205 turns of 0.6 mm diameter copper wire wound onto an aluminum bobbin with rectangular fins to aid the dissipation of heat via air cooling. This wire thickness was chosen to keep the current density in the coil below 2 A.mm^{-2} since a general rule of thumb given is that anything above this current density would require water cooling. The fins fit into the arms of a perspex frame which is bolted to the conversion flange such that the coils are held either side of the trapping cell. There is a 27 mm diameter hole through each of the bobbins to allow for molasses beams to pass through to the trapping cell. Oppositely directed currents are applied to the coils. This results in a Maxwell gradient magnetic field being produced with its zero point near the center of the trapping cell.

To measure the magnetic field a Gauss probe was attached to a translation stage and moved along the central axis between the two coils. A current of 500 mA was applied to both coils. Readings from the Gauss meter were taken every 1 mm along the central axis.

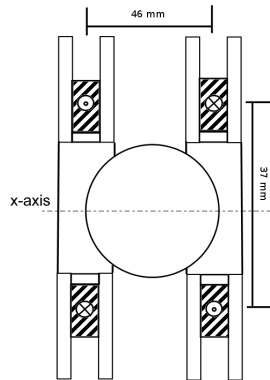


Figure 3.4: Illustration of the magnetic coils and spherical trapping cell. The coil area is represented by hatch lines. Current directions and dimensions of coils as indicated.

Chapter 4 - RESULTS AND DISCUSSION

4.1 Characterisation of External Cavity Diode Lasers

The turn on curves of laser optical output power versus current for the re-pump and trapping lasers used are shown in figures 4.1 and 4.2 respectively. For the re-pump laser measurements, the current was limited to 110 mA and a maximum output power of 27.26 mW was achieved. This is more than sufficient operating power according to Wieman et al. [11] to perform laser cooling and trapping. The threshold current is found by plotting two trend lines, one through the data before lasing occurs and one through the data after lasing is achieved and then setting the two equations equal to each other and solving for x . The threshold current is 32.77 mA. The slope efficiency (gradient of the linear increase) is 0.35 mW.mA^{-1} . Previous measurements done by G.N.Botha [3] on the home built re-pump ECDL show the threshold current as 31.09 mA and the power at maximum injection current (125.5 mA) as 11 mW. The slope efficiency is given as 0.117 mW.mA^{-1} .

In application to laser cooling the quality of the beams are largely irrelevant and therefore not discussed [11].

The re-pump ECDL has a Littrow configuration. This configuration has the problem that the beam steers when the frequency is tuned. The geometry however has been designed to maximise the mode-hop free tuning range, but no fine tuning of the geometry is possible.

For the trapping ECDL, the threshold current is 31.83 mA and the slope efficiency is 0.48 mW.mA^{-1} .

The trapping ECDL (vortex system) has a Littman-Metcalf configuration [15]. An advantage of this configuration is that the beam does not steer as the laser is frequency tuned and is well optimised for mode-hop free tuning.

The beam steering (amount by which the direction of the laser beam changes when adjusting the voltage to the piezo) for the re-pump laser was tested by directing the beam onto graph paper at a distance of 1720 mm from the aperture of the ECDL. Over the entire piezo voltage range, the change in position of the beam on the graph paper was so small as to not be detectable with the naked eye. If we assume that a change greater than 0.5 mm would have been noticeable, we calculate the change in the angle of the beam as smaller than 0.016° .

It was found that the combination of operating the re-pump laser at 91 mA and setting the temperature of the re-pump laser's temperature controller to 11°C (16°C measured) tunes the laser wavelength to the correct ballpark from which small adjustments of the current may lead to fluorescence being seen in the sample cell and thus indicating that the laser frequency is scanning over

the D_2 lines of Rubidium.

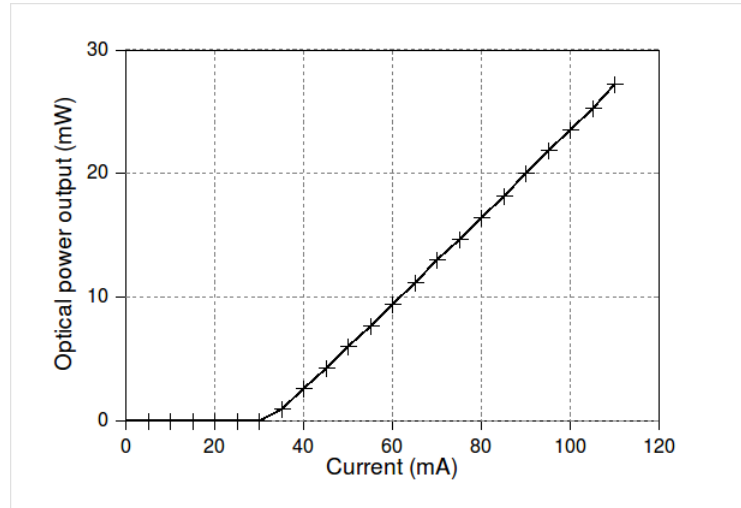


Figure 4.1: Turn on curve of re-pump laser showing a maximum power of 27.26 mW (at 110 mA) operated at 21.6°C. The threshold current is 32.77 mA. The slope efficiency is $0.35 \text{ mW}\cdot\text{mA}^{-1}$. These values are obtained by applying linear fits to the data before and after the threshold. The fits are not shown.

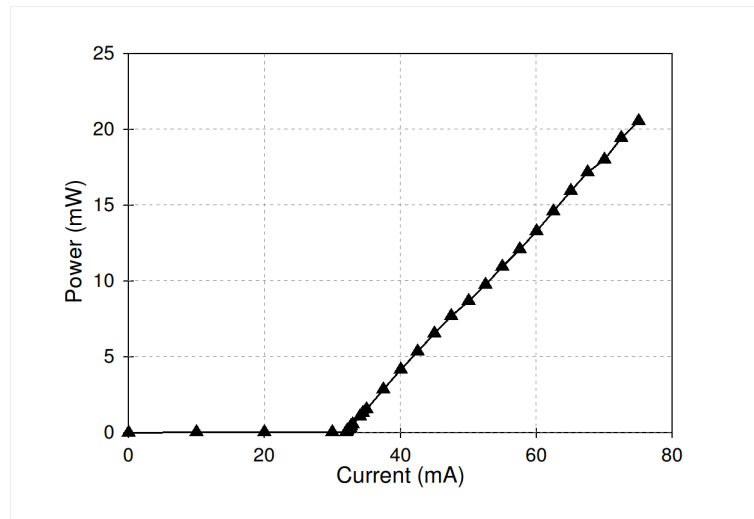


Figure 4.2: Turn on curve of trapping laser (vortex system) showing a maximum power of 20.75 mW. We did not measure the operating temperature as this required linking the laser system to a computer and running diagnostic software. The threshold current is 31.83 mA. The slope efficiency is $0.48 \text{ mW}\cdot\text{mA}^{-1}$. These values are obtained by applying linear fits to the data before and after the threshold. The fits are not shown.

4.2 Optical Setup Characterisation

4.2.1 Optical power

The Vortex external cavity diode laser was operated at a current of 74.8 mA. The optical power at various points in the setup was measured. The total power output of the laser was 20.4 mW. The light then passes through an optical isolator and 18.9 mW of power was measured. Approximately 6% (1.14 mW) of the total laser light after the optical isolator is split off to the saturated absorption spectroscopy (SAS) setup. The laser power in the two probe beams are 0.07 mW and 0.04 mW respectively. A power of 0.57 mW enters the sample cell as the pump beam.

15.75 mW of light is transmitted to the trapping line after the SAS light is split off. The beam goes through a $\frac{\lambda}{2}$ plate where the polarisation may be adjusted before a total of 11.5 mW enters the Glan-Taylor prism. The orientation of the $\frac{\lambda}{2}$ plate may be adjusted so that anywhere from 0.05 mW to 10 mW (0.4 % to 87 %) of the light is transmitted. A suitable balance was found with 7 mW of power transmitted and 3.7 mW of power reflected at the air interface of the first Glan-Taylor prism.

The 7 mW of light is split when it encounters a non-polarising beam splitter plate. The power ratio of the 2 resulting beams cannot be adjusted and is typically 1.35 : 1.

Approximately 3 mW of laser power enters the trapping cell in each of the three beams of the optical molasses.

Up to 1 mW of power may be lost by the time the retro-reflected beams enter the trapping cell (calculated from losses observed on initial passes through optical elements).

For the re-pump ECDL an operational power level of 22.13 mW was achieved at a diode current of 91 mA.

After a portion of the beam is split off to a saturated absorption spectroscopy setup, the beam is directed through a $\frac{\lambda}{2}$ plate so that the percentage of re-pump light that is reflected at the Glan-Taylor prism may be controlled. A total of 5.83 mW of power in the re-pump beam enters this second Glan-Taylor prism where it is combined into the beam line.

4.2.2 Polarisation

During the propagation of the light through the various optical elements, it undergoes changes in its polarisation. It is important to keep track of the polarisation of the light in order to manipulate it to the proper purpose. The polarisation of the light can be described mathematically with the aid of Jones matrix calculations. After leaving the optical isolator, the light is linearly polarised at 45° from the horizontal x -axis. Let z be the propagation direction of the light. This is expressed by the Jones matrix [17].

$$\frac{1}{\sqrt{2}} \begin{bmatrix} 1 \\ 1 \end{bmatrix} \quad (4.1)$$

The light then encounters a half-wave plate which has the Jones matrix expression

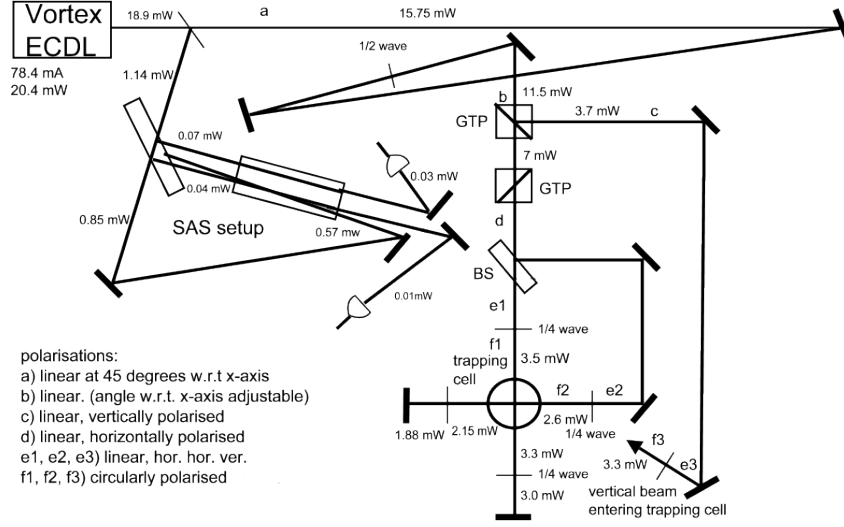


Figure 4.3: Illustration of optical setup for trapping ECDL showing trapping laser power only at various points. The trapping ECDL was operated at 74.8 mA and produced 20.4 mW of laser output. The optical isolator directly after the laser aperture is not shown. The re-pump laser (not shown) is included into the beam line at the second beam-splitter cube. The lenses used for beam expansion are also not shown.

$$\begin{bmatrix} \cos 2\theta & \sin 2\theta \\ \sin 2\theta & -\cos 2\theta \end{bmatrix}, \quad (4.2)$$

where θ is the angle made by the fast axis w.r.t. the horizontal x -axis. It is possible to adjust the angle to control the ratio of vertical and horizontal polarised light. For example if we were to set θ to 15° then our resultant linear polarisation would be given by

$$\frac{1}{\sqrt{2}} \begin{bmatrix} \cos(30) & \sin(30) \\ \sin(30) & -\cos(30) \end{bmatrix} \begin{bmatrix} 1 \\ 1 \end{bmatrix} = \frac{1}{\sqrt{2}} \begin{bmatrix} \frac{1+\sqrt{3}}{2} \\ \frac{1-\sqrt{3}}{2} \end{bmatrix} = \begin{bmatrix} 0.966 \\ -0.259 \end{bmatrix} \quad (4.3)$$

which means that more light would have polarisation along the horizontal x -axis than along the vertical y -axis. Thus when encountering a Glan-Taylor prism (which we may treat mathematically as two separate and independently acting instances of a linear polariser with its axis of transmission aligned horizontally and vertically respectively) the horizontally and vertically polarised light will be separated into two beams, the respective intensities of the beams depending on the orientation of the $\frac{\lambda}{2}$ plate (described by the angle θ in expression 4.2). In this way the power ratio of the vertical and two horizontal trapping beams may be controlled.

The vertical trapping beam is polarised linear and vertically, the horizontal beams linear and horizontally. The second Glan-Taylor prism and the non-polarising beam splitter splitting the 2 horizontal trapping beams do not change the polarisation.

During each stage of splitting from the laser output to exiting the trapping cell, the intensity and polarisation of the separate trapping and re-pump beams were measured and recorded.

In the experiment as shown in figure 3.3, the light that is reflected at the air interface of the first Glan-Taylor prism is vertically polarised. This light is directed by the optics to become the vertical molasses beam. The light transmitted through the first Glan-Taylor prism is horizontally polarised. Subsequently passing through the second Glan-Taylor prism (where the re-pump light is combined to co-propagate along the main beam line) will have no effect on the polarisation of the light as it will simply be transmitted again. This light then meets a non-polarising beam splitter which splits the beam into what becomes the two horizontal molasses beams which both consist of horizontally polarised light. The three molasses beams each pass through their own set of quarter wave plates before and after the trapping cell. These convert the linearly polarised light into circularly polarised light. The orientation of the first quarter wave plate a beam encounters relative to the magnetic field that is produced by the Maxwell gradient coils is important. The second wave plate's rotation is not important as at any orientation two passes by the beam through it (second pass occurs after retro-reflection) will result in the opposite circular polarisation to the original incident beam. The two beams which propagate through the cell perpendicular to the magnetic coil axis should have the same circular polarisation, while the beam which propagates along the coil axis should have opposite circular polarisation as described by Wieman [11]. In order to achieve the correct relative polarisations the orientation of the fast axis of the quarter wave plates must be set according to the linear polarisation of the beam.

For the horizontal non-coaxial beam, the axis is set at 45° counter-clockwise with respect to the linear polarisation when looking into the laser beam (this produces light with a clockwise polarisation sense).

The nature of our setup forced us to have a reflection from a mirror at 45° incidence angle after the first quarter wave plate in the vertical beam. This has the important result that the axis of the first quarter wave plate in the vertical arm must be oriented 45° clockwise with respect to the linear polarisation when looking into the beam (this produces light with a clockwise polarisation sense after reflection at the 45° mirror). For the remaining horizontal coaxial beam the axis of the quarter wave plate is oriented 45° clockwise with respect to the linear polarisation (this produces light with a counter-clockwise polarisation sense).

An experiment was conducted to confirm the effect the reflection from the 45° mirror has on the polarisation sense of the light. Firstly the beam, being linearly polarised, was sent through a half wave plate to adjust it to be horizontally polarised. This was done by sending the resulting light through a Glan-Taylor prism and measuring the power transmitted. The half wave plate's orientation was adjusted until a maximum power transmission was seen. Then a quarter wave plate is added into the beam with its fast axis at 45° clockwise relative to the horizontal x-axis when looking into the beam. This produces counter-clockwise polarised light (had the light been vertically polarised, the quarterwave plate would have converted it to clockwise polarised light). In part a) of figure 4.4, passing the beam through a second quarter wave plate with its

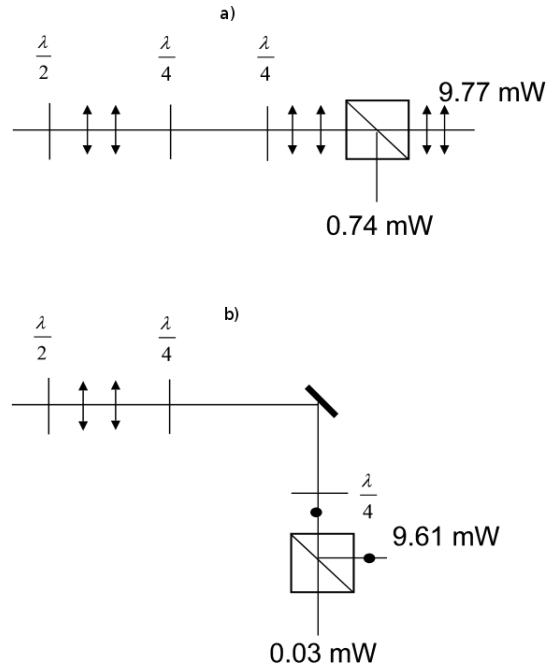


Figure 4.4: Testing the effect of 45° mirror on the polarisation sense. From a) to b) the orientation of the fast axis of the quarter wave plates with respect to the horizontal x-axis was not changed.

fast axis at 45° counter-clockwise relative to the horizontal x-axis when looking into the beam converts the light back to horizontally polarised as evidenced by the high percentage of power transmitted through the Glan-Taylor prism. In part b) the light is reflected off of a 45° mirror after being sent through the first quarter wave plate. It is then directed onto the second quarter wave plate with its fast axis at 45° counter-clockwise relative to the horizontal x-axis when looking into the beam. The light is converted to vertically polarised light as evidenced by the high percentage of it that is reflected at the Glan-Taylor prism. The conclusion for this change in resulting polarisation is that at the 45° mirror, circularly polarised light undergoes a phase change such as to change its polarisation sense from clockwise to counter-clockwise or vice versa.

4.3 Magnetic Field Characterisation

Simulations by Ithemba labs [18] (having the same coil characteristics as used in the experiment at 500 mA) show that the coils produce a linear gradient magnetic field around the origin, along the central axis with a gradient of 16.4 $\text{G}\cdot\text{cm}^{-1}$ (figure 4.5) as well as along a transverse axis with a gradient of 7.7 $\text{G}\cdot\text{cm}^{-1}$ (figure 4.6).

Figure 4.7 shows the magnetic field value measured along the the central axis between the two coils when 500 mA of current is sent through them. The gradient is fairly linear and sufficient for the purposes of creating a magneto optical trap. Of most interest is the range of ± 5 mm (related to the diameter

of trapping beams) around the zero point of magnetic field as this will form the center of the trap. A linear fit to the data has a gradient of 17.2 G.cm^{-1} . This is also sufficient to create a trap according to Wieman [11] and may be adjusted by adjusting the current through the coils. The gradient and linearity along the central axis agree well between the measurement and simulation. Although the gradient along the transverse axis is less than half, this should not have a crippling effect on the performance of the trap.

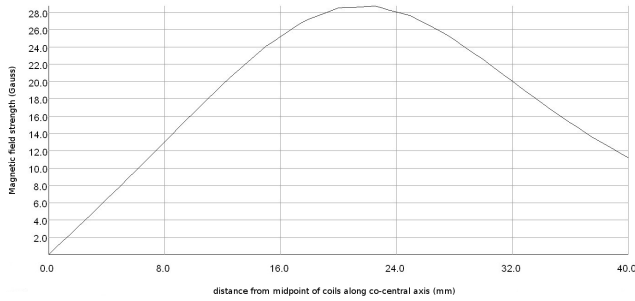


Figure 4.5: Graph of simulated magnetic field strength versus position between coils along central axis courtesy of Ithemba labs [?]. The graph is anti-symmetric about the origin. Only the linear range from 0 mm to 5 mm is important. The gradient in this region is 16.4 G.cm^{-1} .

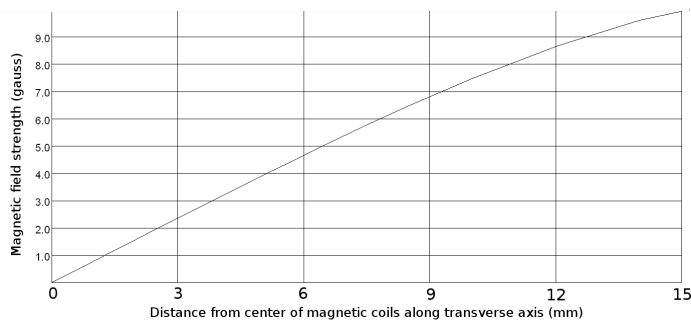


Figure 4.6: Graph of simulated magnetic field strength versus position between coils along transverse axis courtesy of Ithemba labs [?]. The graph is anti-symmetric about the origin. The linear range from 0 mm to 5 mm is of most interest. The gradient in this region is 7.7 G.cm^{-1} .

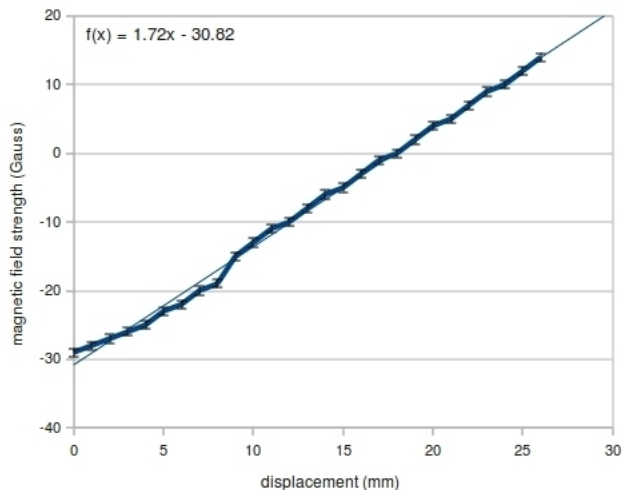


Figure 4.7: Graph of measured magnetic field strength versus position between coils along central axis. The zero of the x-axis is taken from an arbitrary point. Of most interest is the linear range from 13 mm to 23 mm. The gradient in this region is 17.2 G.cm^{-1} .

4.4 Saturated Absorption Spectra of Rubidium

Since the pump beam has approximately 15 times more power than the probe beam with which it overlaps, it will saturate the absorption for all atoms that see the same Doppler shifted frequency of the two beams, i.e. those atoms that have a zero velocity component along the axis of the beams. The saturation causes a higher transmission of the pumped probe beam when compared to the unpumped probe beam when the laser frequency is within the Doppler-free line width from a rubidium absorption line. Figure 4.8 shows the Doppler broadened absorption peaks of ^{87}Rb and ^{85}Rb (above). It demonstrates that the Vortex ECDL can scan over $\pm 13 \text{ GHz}$ without experiencing a mode-hop (The nature of the tuning with the re-pump laser made it impossible to determine over what bandwidth region could be tuned without experiencing a mode hop). Hyperfine structure not resolved, the FWHM of the $5S_{1/2}F = 1 \rightarrow 5P_{3/2}F' = X$ line as taken from the graph is 0.6252 GHz . the FWHM of the $5S_{1/2}F = 2 \rightarrow 5P_{3/2}F' = X$ line as taken from the graph is 0.5982 GHz . The graphs below in figure 4.8 show the SAS of the ^{87}Rb lines, Doppler free, with hyperfine lines resolved. The difference signal as a function of frequency shows a Doppler-free spectrum of the hyperfine splitting of the ^{87}Rb lines (see figure 4.8).

Crossover peaks also occur in these results. They are spaced exactly in the middle of two spectral lines. They are the result of atoms that have a velocity such that they see the probe beam Doppler shifted to the one spectral line and the pump beam Doppler shifted to the other spectral line. Since the two transitions have a common lower quantum state, saturation occurs. The literature values of the frequency for the lines were used for relative frequency

calibration of the results. The values for the relative frequency were plotted against the pixel position of the peaks as read from the oscilloscope data and are shown in figures 4.10 and 4.12. The linearity of these plots confirms that a linear calibration should be used.

Figure 4.9 shows the saturated absorption signal of the $5S_{1/2}F = 2 \rightarrow 5P_{3/2}F' = X$ hyperfine lines of ^{87}Rb . There are three hyperfine lines and 3 crossover peaks. The FWHM of the trapping line $5S_{1/2}F = 2 \rightarrow 5P_{3/2}F' = 3$ as shown in figure 4.9, is 22.68 MHz. The frequency range to which the laser could be locked is approximately 10 MHz. The probable detuning when locked (assuming locking occurs on the steepest part of the slope) is approximately 11 MHz.

Figure 4.11 shows the saturated absorption signal of the $5S_{1/2}F = 1 \rightarrow 5P_{3/2}F' = X$ hyperfine lines of ^{87}Rb . There are three hyperfine lines and 3 crossover peaks.

The FWHM of the re-pump line $5S_{1/2}F = 1 \rightarrow 5P_{3/2}F' = 2$ as shown in figure 4.11, is 22.6 MHz.

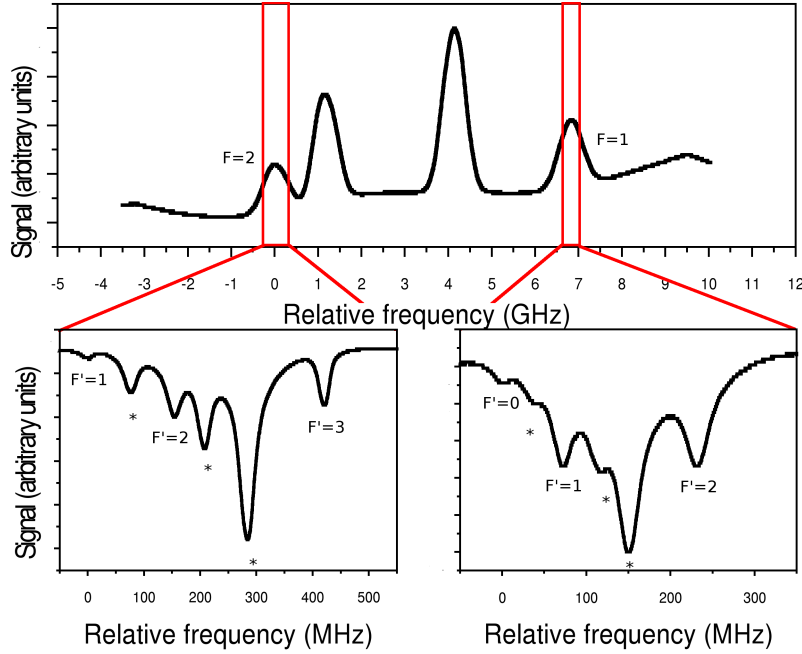


Figure 4.8: The Doppler broadened fine structure of Rubidium D2 line for ^{87}Rb and ^{85}Rb (above) and the hyperfine structure of the ^{87}Rb lines (both below).

4.5 Results on Frequency Locking of External Cavity Diode Lasers

Once fluorescence is seen in the Rubidium sample cells used in the saturated absorption setup, the side-lock servo system is used to zoom into the required hyperfine line and lock the laser frequency to it. For a detailed guide to the

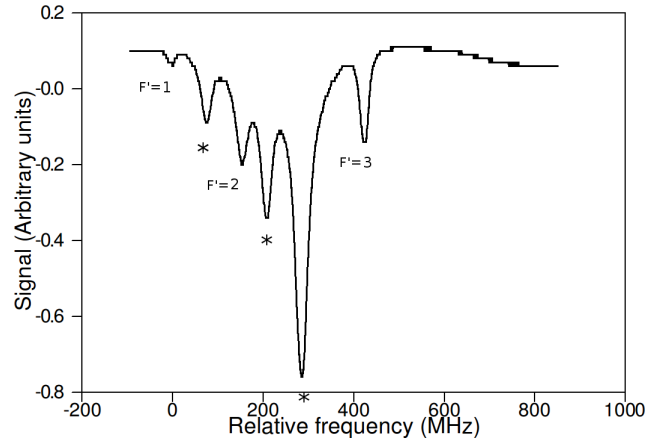


Figure 4.9: Saturated absorption signal of the hyperfine structure of the $5S_{1/2}F = 2 \rightarrow 5P_{3/2}F' = X$ line for ^{87}Rb . The transition to $F' = 3$ is used for trapping. Peaks marked with an asterisk are crossover peaks.

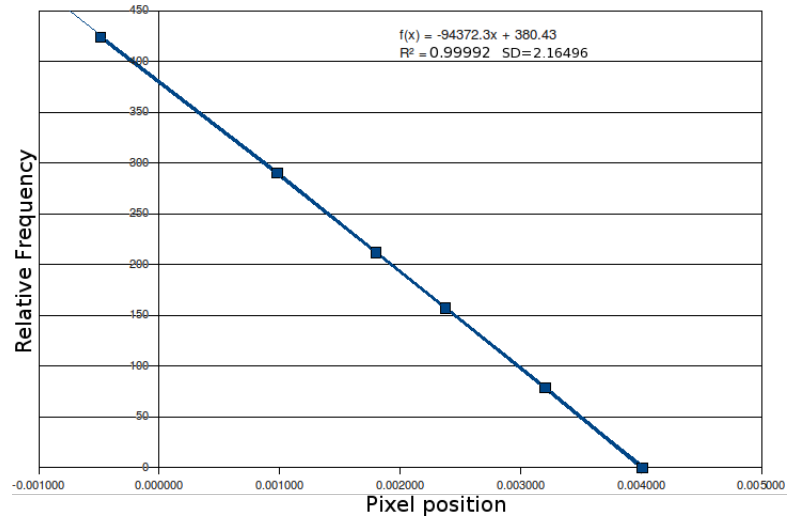


Figure 4.10: Calibration plot for the $5S_{1/2}F = 2 \rightarrow 5P_{3/2}F' = X$ line. The relative frequency (MHz) of the peaks are plotted against their pixel position as given by the oscilloscope. The equation for the linear fit is shown.

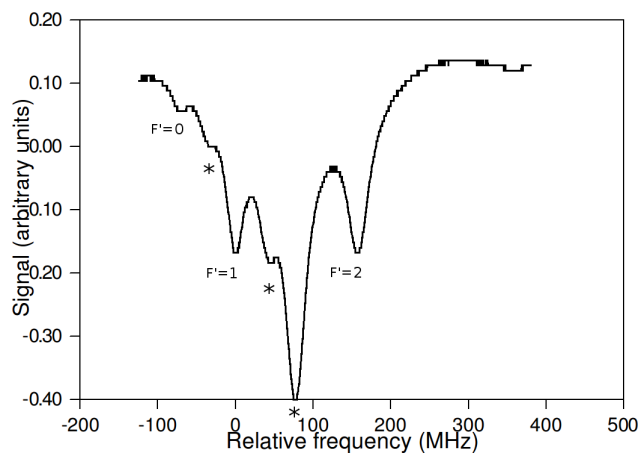


Figure 4.11: Saturated absorption signal of the hyperfine structure of the $5S_{1/2}F = 1 \rightarrow 5P_{3/2}F' = X$ line for ^{87}Rb . The transition to $F' = 1$ or $F' = 2$ is used for trapping. Peaks marked with an asterisk are crossover peaks.

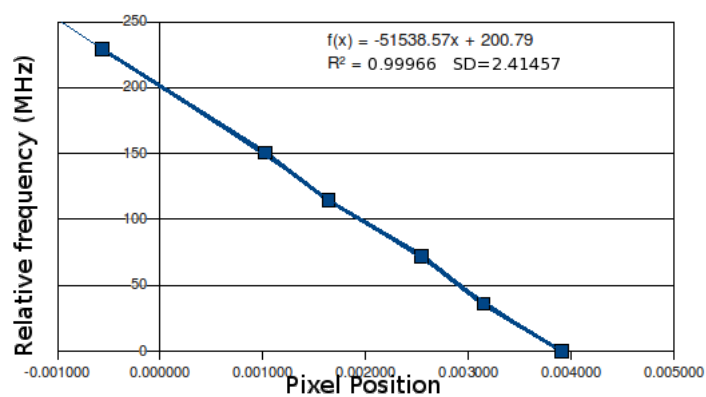


Figure 4.12: Calibration plot for the $5S_{1/2}F = 1 \rightarrow 5P_{3/2}F' = X$ line. The relative frequency (MHz) of the peaks are plotted against their pixel position as given by the oscilloscope. The equation for the linear fit is shown.

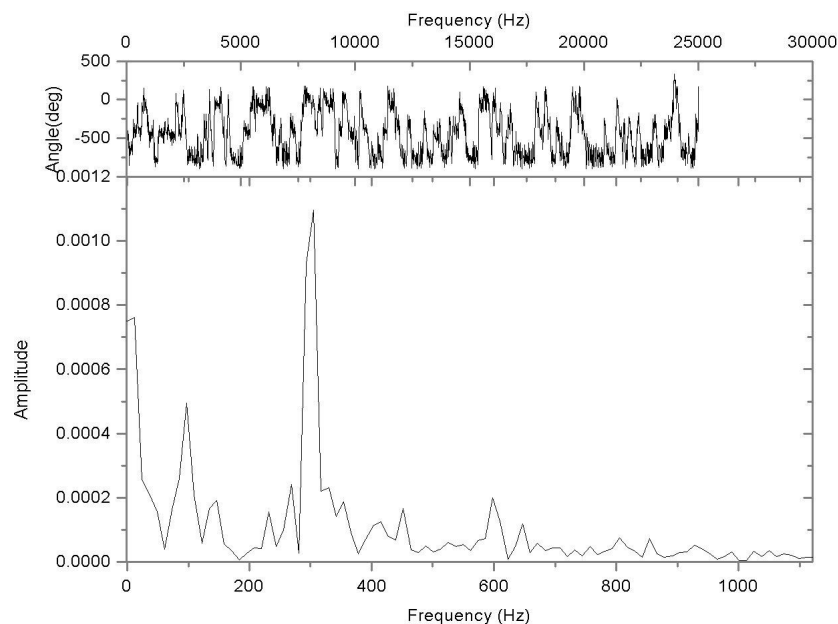


Figure 4.13: Fast Fourier transform of error signal of vortex laser in locking.

locking procedures w.r.t. the side lock servo system, one may consult the masters thesis by G.N.Botha [3].

The lasers are locked to the low frequency (red) slope of the relevant hyperfine line. The lockable frequency range of this slope is approximately 10 MHz and the typical detuning of the laser once locked is 11 MHz (assuming the laser is locked to the steepest part of the slope).

If left undisturbed the laser may stay in locking for days at a time. The laser locking can also endure reasonable vibrations generated from working on the optical table, walking around and sound vibrations (such as conversations or playing music) in the lab.

A fast Fourier transform of the error signal exhibited on the oscilloscope when the vortex laser is in locking is shown in figure 4.13. Peaks are seen around 60 and 250 Hz. It is not known what causes this noise, but it is less than 5 percent of the amplitude of the peak used for locking, and therefore deemed negligible.

4.6 Magneto Optical Trap Operation

To date, trapping has not yet been demonstrated in our setup. Fluorescence from Rubidium atoms was shown in the spherical trapping cell meaning that appropriate vacuum level had been reached, sufficient Rb vapor was introduced into the system and sufficient laser light from both the trapping and re-pump lasers at the appropriate wavelengths was directed into the cell to form the optical molasses. At the time fluorescence was demonstrated, the orientation of the quarter wave plates was incorrect, preventing the formation of a magneto optical trap. However shortly afterward the ion pump ceased to function and

thus we were no longer able to achieve the required vacuum levels for the experiment to continue. At time of writing the ion pump is away for repairs.

Chapter 5 - SUMMARY, CONCLUSIONS AND FUTURE WORK

A summarized study of the physical principles of laser cooling and trapping of neutral atoms with specific focus on Rubidium 87 was performed. The effect of the trapping parameters on the number of trapped atoms was studied from literature. The existing incomplete vacuum system [3] was redesigned and painstakingly rebuilt to decrease the overall vacuum chamber volume and improve the ultimate pressure to the order of 10^{-7} mbar. A trapping cell was designed and implemented into the vacuum system. A mount for the getter to act as a source of atomic Rubidium was designed, implemented into the vacuum system and demonstrated to perform sufficiently. Magnetic coils to provide a linear gradient magnetic field in the trapping cell to add Zeeman degeneracy for sub-Doppler cooling were designed, constructed, characterised and implemented. The previously existing home-built ECDL and newly commercially acquired vortex ECDL were characterised and incorporated into the optical setup which was essentially broken down, redesigned and rebuilt from scratch to form an optical molasses inside the trapping cell capable of sub-Doppler cooling. The optics and electronics for a second saturated absorption spectroscopy and frequency locking setup were built our department electrician. Saturated absorption spectroscopy and frequency locking was performed with both lasers and the fine and hyperfine structure of the ^{87}Rb spectrum investigated.

We have thus successfully constructed a complete system capable of laser cooling and trapping of atoms. Significant experience with the various equipment has been obtained. At present, trapping has not yet been demonstrated, but this is largely due to time limitations and untimely equipment failure. As a result the effect of the trapping parameters on the number of trapped atoms was not experimentally investigated.

It is our hope that this system will lead to more research into ultra cold atoms at the University of Stellenbosch.

5.1 Proposed Future Work

It is possible to expand the MOT system to perform evaporative cooling and produce a Bose-Einstein condensate. This would possibly involve a MOT transfer system whereby trapped atoms could be transported to a secondary trap constructed in an adjacent vacuum system in a similar fashion to that of the Lewandowski group [5].

Plans are in place to do collaborative work with researchers from theoretical

physicists from Stias on the behavior of trapped atoms. There is also talk of collaboration with the femtosecond and fiber laser groups at Stellenbosch University to devise an experiment to probe atom behavior in the femtosecond regime.

Chapter 6 - APPENDIX

6.1 Vacuum System Start-Up Procedure

To pump down the vacuum system from atmospheric pressure the following steps and checks should be performed:

1. Turn on pressure gauge meter and turbo pump controller. Check that there are no error messages and that the turbo pump controller reads “pump on standby”.
2. Make sure all three valves are open.
3. Turn on roughing pump. Note that the pressure drops according to the pressure gauge.
4. At approximately one millibar, start the turbo pump.
5. The pressure should continue to drop as the turbo pump approaches operating speed of 32000 RPM.
6. After approximately 24 hours of pumping, start the ion pump.
7. If the “high load” light on the ion pump controller is on, there is still too much pressure for the ion pump to properly start and it should be turned off and an attempt made to start it again at a later time.
8. When the ion pump is properly running, the column of lights should be partially lit and the pressure may be determined by comparing the current reading to the pressure value on the graph supplied by the manufacturer.
9. At this point the metal angle valve may be closed and the ion pump should maintain the vacuum level.

6.2 Circular Polarisation of Light

This section is meant to give the reader a basic conceptualisation of how to think about and use circularly polarised light with regards to laser cooling.

Circularly polarised light has a non-zero angular momentum. When a photon is absorbed by the atom, this angular momentum must be stored due to the conservation of angular momentum.

Consider an atom in free space so that no external torques act upon it. It's total angular momentum is given by the vector \mathbf{J} . Typically \mathbf{J} is the total angular momentum produced by the coupling of the orbital angular momentum \mathbf{L} and the spin angular momentum \mathbf{S} , as expressed by $\mathbf{J} = \mathbf{L} + \mathbf{S}$.

The hyperfine structure is a result of the coupling of \mathbf{J} with the total nuclear angular momentum \mathbf{I} . The total atomic angular momentum \mathbf{F} is then given by

$$\mathbf{F} = \mathbf{J} + \mathbf{I} \quad (6.1)$$

The magnitude of \mathbf{F} can have the values

$$|J - I| \leq F \leq J + I$$

The total angular momentum maintains a fixed magnitude J and a fixed z component J_z [19]. The magnitude and z component of the total angular momentum \mathbf{J} are specified by the two quantum numbers j and m_j according to the following quantisation conditions

$$J = \sqrt{j(j+1)}\hbar \quad (6.2)$$

$$J_z = m_j\hbar \quad (6.3)$$

The possible values of the quantum number m_j are

$$m_j = -j, -j + 1, \dots, +j - 1, +j \quad (6.4)$$

\mathbf{J} is associated with the magnetic dipole moment

$$\vec{\mu}_j = \frac{-g_j\mu_B\mathbf{J}}{\hbar} \quad (6.5)$$

which has magnitude

$$\mu_j = g_j\mu_B\sqrt{j(j+1)} \quad (6.6)$$

and z component

$$\mu_{jz} = -g_j\mu_B m_j \quad (6.7)$$

where g_j is the Landé g-factor and $\mu_B = \frac{e\hbar}{2m}$

We are only interested in the transitions caused by circularly polarised light.

σ^+ polarised light is defined as light which possesses the angular momentum required to cause a transition in which the delta of the quantum number m_j from the ground state to the excited state is $+1$. Similarly σ^- polarised light is defined as light which possesses the angular momentum required to cause a transition in which the delta of the quantum number m_j from the ground state to the excited state is -1 .

The simplest case is if we assume the ground state to have $J' = 0$ and the excited state to have $J'' = 1$. Thus the ground state has $m_j = 0$ and we are exciting into either the $m'_j = -1$ (via σ^- polarised light) or $m'_j = +1$ (via σ^+ polarised light) states. If no external magnetic field is applied the states $m'_j = -1$ and $m'_j = +1$ have the same energy and the transition energy from the ground state is also the same. According to the Zeeman effect, the energy states will lose this degeneracy if an external electric field is applied, with the change in energy of each energy state given by $\Delta E = -\vec{\mu} \cdot \mathbf{B}$. Assume a linear gradient magnetic field is applied such that there is a linearly increasing magnetic field on the right hand side of the origin, zero magnetic field at the

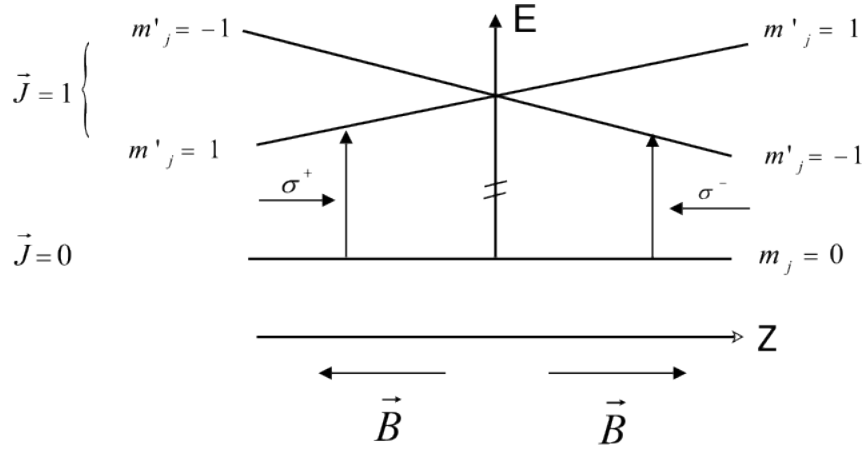


Figure 6.1: A sketch of the splitting of the energy levels by the Zeeman effect and the circularly polarised light required for the lower energy transition.

origin and linearly decreasing magnetic field such that the magnetic field is zero at the origin, its magnitude increases linearly with distance from the origin, and its directions on the left and right of the origin are always opposing. In a MOT there will be an axis with \mathbf{B} fields pointing away from the origin and 2 axes with \mathbf{B} fields pointing towards the origin or vice versa. Consider a \mathbf{B} field gradient with \mathbf{B} fields pointing away from the origin as in figure 6.1. Choose the z -axis left to right as indicated in the figure. It is convention to represent the \mathbf{B} field directions by signs where a “positive” \mathbf{B} field means pointing into the positive z -direction.

In this specific magnetic field the energy levels of $m'_j = -1$ and $m'_j = +1$ will be perturbed as shown in figure 6.1. On the right hand side of the origin in figure 6.1 the \mathbf{B} -field is in the positive z -direction. The energy splitting is calculated

$$\Delta E = -\vec{\mu}_j \cdot \mathbf{B}$$

$$\Delta E = -\vec{\mu}_j \cdot (|\mathbf{B}|\hat{z})$$

$$\Delta E = -|\mathbf{B}|\vec{\mu}_j \cdot \hat{z}$$

$$\Delta E = -|\mathbf{B}|\mu_{jz}$$

$$\Delta E = -|\mathbf{B}|(-g_j\mu_B m_j)$$

$$\Delta E = |\mathbf{B}|(g_j\mu_B m_j)$$

so that the sub-level with $m'_j = -1$ has the lowest energy in the upper state (for g_j positive).

On the left hand side of the origin in figure 6.1 the \mathbf{B} -field is in the negative z -direction. However μ_{j_z} and m_j are defined in terms of the z -axis and not the \mathbf{B} -field direction and thus do not change.

Therefore

$$\Delta E = -\vec{\mu}_j \cdot \mathbf{B}$$

$$\Delta E = -\vec{\mu}_j \cdot (-|\mathbf{B}|\hat{z})$$

$$\Delta E = |\mathbf{B}|\vec{\mu}_j \cdot \hat{z}$$

$$\Delta E = |\mathbf{B}|\mu_{j_z}$$

$$\Delta E = -|\mathbf{B}|\mu_B m_j$$

so that the sub-level with $m'_j = +1$ has the lowest energy.

If we red-detune the laser light we find that on both sides of the figure, the transition to the state with the lower energy is more likely. On the right hand side, this is the transition to the $m'_j = -1$ state via σ^- polarised light. On the left hand side, this is the transition to the $m'_j = +1$ state via σ^+ polarised light.

We already know that the atom receives a small momentum kick in the direction of the photon's propagation when it is absorbed. Since we wish to use this to create a position dependent force that tends to move the atom towards the origin, we must have σ^- polarised light impinging on the atom from the left hand side and σ^+ impinging on the atom from the right hand side as shown in figure 6.1.

In order to induce circular polarisation in light that is linearly polarised, we send it through a quarter wave plate. The circularly polarised light that results is either clock wise or counter clock wise in nature when looking into the laser beam. Using the right hand rule one may determine the direction of the angular momentum associated with the light. In order to determine the orientation of the fast axis of the quarter wave plate one must determine what direction of angular momentum is required to induce the desired value for $\Delta m_j = m'_j - m_j$.

In the figure 6.2 light having an angular momentum $\vec{\Omega}$ towards the left may cause a transition having a $\Delta m_j = -1$. If this light is propagating towards the right it is clockwise in nature. If the light is propagating towards the left it is counter-clockwise in nature.

Similarly light having an angular momentum towards the right may cause a transition having a $\Delta m_j = +1$. If this light is propagating towards the right it is counter-clockwise in nature. If the light is propagating towards the left it is clockwise in nature.

For the trap (with this particular orientation of the magnetic field gradient) it is required that light impinging on the atom from the left is σ^- polarised

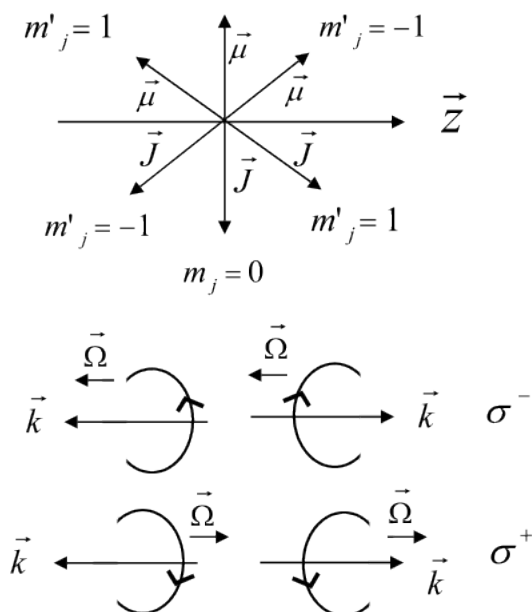


Figure 6.2: Illustration of the relation between angular momentum of light, its σ polarisation and its polarisation sense.

and thus has a clockwise polarisation sense and light impinging from the right is σ^+ polarised and thus also has a clockwise polarisation sense. The reason for the polarisation senses being the same is that the direction of propagation has changed, as well as the direction of the required angular momentum and these two changes cancel out to give the same polarisation sense.

Since we want to use the retro-reflections of the laser beams to form half of the molasses, we must investigate how retro-reflection affects the polarisation sense. Assume that we have clockwise circularly polarised light propagating to the right onto a mirror as in figure 6.3. In this figure the y-component of the electromagnetic wave leads the x-component by 90° . Upon reflection at the mirror, both the x and y-components undergo a 180° phase change.

Now the light is propagating towards the left and has a counter-clockwise polarisation sense.

Of course we want the reflected light to have clockwise polarisation sense instead (and thus opposite angular momentum to the original incident light), so we insert a quarter wave plate into the path of the beam. Two passes through the quarter wave plate will retard one of the components by a total of 180° producing the required clockwise polarisation sense.

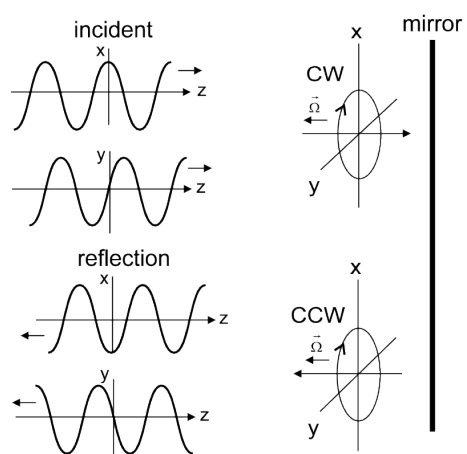


Figure 6.3: Illustration showing what happens to the polarisation sense during retro-reflection

Bibliography

- [1] Daniel A. Steck, “Rubidium 87 D Line Data”, available online at <http://Steck.us/alkalidata> (revision 2.1.2, 12 August 2009)
- [2] <http://www.files.chem.vt.edu/chem-ed/spec/atomic/theory/lifetime.html>
- [3] G.N.Botha, “Development of an external cavity diode laser for application to spectroscopy and laser cooling and trapping of rubidium”, Master’s thesis, University of Stellenbosch, 2008
- [4] <http://www.chemistryexplained.com/elements/P-T/Rubidium.html#ixzz14D6WEs7y>
- [5] H. J. Lewandowski, “Simplified System for Creating a Bose–Einstein Condensate” *Journal of Low Temperature Physics*, Vol. 132, Nos. 5/6, September 2003
- [6] David R. Lide, editor *CRC Handbook of Chemistry and Physics 77th . Edition*. CRC Press, 1996-1997.
- [7] D. Sesko, C. Fan, C. Wieman, “Production of a cold atomic vapor using diode-laser cooling”, *J. Opt. Soc. Am. B*, **5**, 1225 (1988).
- [8] S. Chu et al., “Three-dimensional viscous confinement and cooling of atoms by resonance radiation pressure”, *Phys. Rev. Lett.* **55**, 48 (1985).
- [9] H.J. Metcalf, P. Van Der Straten, “Laser cooling and trapping”, Springer-Verlag New York (2002)
- [10] R. Loudon, “The quantum theory of light”, Oxford University press, (2000)
- [11] C. Wieman, G. Flowers, S. Gilbert, “Inexpensive laser cooling and trapping experiment for undergraduate laboratories”, *American Journal of Physics* **63** (4), 317–330 (1995)
- [12] R.R. Silva, K.M.F. Magalhães, E.A.L. Henn, L.G. Marcassa, V.S. Bagnato, “Temperature determination for magneto optical trapped atoms using a single parameter transient absorption” *Optics coms.* **265**, 526-531 (2006).
- [13] W. D. Phillips, “Laser cooling and trapping of neutral atoms”, *Reviews of Modern Physics*, Vol. 70, No. 3, July 1998
- [14] K.B. MacAdam, A. Steinbach, C. Wieman, “A narrow-band tunable diode laser system with grating feedback and a saturated absorption spectrometer for Cs and Rb,” *Am. J. Phys.* **60**, 1098-1111 (1992).

- [15] User's guide, Tunable diode laser 7000/6000, New Focus™ a division of Bookham
- [16] G.P. Nyamunda, "Design and development of an external cavity diode laser for laser cooling and spectroscopy applications", Master's thesis, University of Stellenbosch, 2006
- [17] Eugene Hecht, "Optics", 3rd edition, Addison-Wesley, (1998), ISBN 0-201-30425-2
- [18] Ithemba LABS, Somerset West, Western Cape, South Africa.
- [19] R. Eisberg, R. Resnick, "Quantum physics of atoms, molecules, solids, nuclei and particles"
- [20] V.S. Letokhov, "Laser control of atoms and molecules", Oxford University press, 33-34 (2007)
- [21] <http://www.files.chem.vt.edu/chem-ed/spec/atomic/theory/lineshap.html>
- [22] <http://massey.dur.ac.uk/research/magnetometry/RbD2line/RbD2line.html>